nature biomedical engineering

ARTICLES

https://doi.org/10.1038/s41551-021-00788-9

Check for updates

Application of prime editing to the correction of mutations and phenotypes in adult mice with liver and eye diseases

Hyewon Jang[1,2,13], Dong Hyun Jo[3,13], Chang Sik Cho[4], Jeong Hong Shin[1,2,5,6], Jung Hwa Seo[7,8], Goosang Yu[1,2], Ramu Gopalappa[1], Daesik Kim[9], Sung-Rae Cho[2,7,8], Jeong Hun Kim[4,10,11] ✉ and Hyongbum Henry Kim[1,2,5,6,12] ✉

The use of prime editing—a gene-editing technique that induces small genetic changes without the need for donor DNA and without causing double strand breaks—to correct pathogenic mutations and phenotypes needs to be tested in animal models of human genetic diseases. Here we report the use of prime editors 2 and 3, delivered by hydrodynamic injection, in mice with the genetic liver disease hereditary tyrosinemia, and of prime editor 2, delivered by an adeno-associated virus vector, in mice with the genetic eye disease Leber congenital amaurosis. For each pathogenic mutation, we identified an optimal prime-editing guide RNA by using cells transduced with lentiviral libraries of guide-RNA-encoding sequences paired with the corresponding target sequences. The prime editors precisely corrected the disease-causing mutations and led to the amelioration of the disease phenotypes in the mice, without detectable off-target edits. Prime editing should be tested further in more animal models of genetic diseases.

Prime editing can induce any small-sized genetic change, including insertions, deletions and all 12 possible point mutations, without donor DNA or double strand breaks[1]. There are four types of prime editors (PEs): PE1, PE2, PE3 and PE3b[1]. PE1 and PE2 are composed of a clustered regularly interspaced short palindromic repeats (CRISPR)-associated protein 9 (Cas9) nickase–reverse transcriptase (RT) fusion protein and a prime-editing guide RNA (pegRNA)[1]. PE3 and PE3b consist of PE2 and one additional single guide RNA (sgRNA)[1].

Prime editing has been used in cultured mammalian cells[1,2] and organoids[3], plants[4] and mouse embryos[5] to introduce genetic changes in a targeted manner. Before prime editing can be applied to treat genetic diseases in humans, correction of both pathogenic mutations and phenotypes of animal models of human genetic diseases must first be demonstrated. In this study, we show that prime editors delivered into mouse models of genetic liver and eye diseases can precisely correct the disease-causing mutation, leading to functional improvement.

Results

A mouse model of tyrosinemia and high-throughput evaluation of pegRNAs. As a prototypic disease model for prime-editing-based therapeutic genome editing in adult animals, we first chose a mouse model of hereditary tyrosinemia type 1 (*Fah*$^{mut/mut}$), which is caused by a loss-of-function mutation in the fumarylacetoacetate hydrolase gene (*Fah*)[6,7]. The mouse model contains a homozygous G-to-A point mutation at the last nucleotide of exon 8, which causes exon 8 skipping and results in loss of function of FAH (Fig. 1a). Pharmacological inhibition of 4-hydroxyphenylpyruvate dioxygenase, an enzyme that acts upstream of FAH in the tyrosine catabolic pathway, with 2-(2-nitro-4-trifluoromethylbenzoyl)-1,3-cyclohexanedione (NTBC) reduces the accumulation of toxic metabolites and thus prevents hepatic injury[6]. We and others have used this mouse model for testing various in vivo genome-editing approaches, including methods based on homology-directed repair (HDR)[8,9], microhomology-mediated end joining[10] and base editing[11]. In addition, because hydrodynamic injections have commonly been used to deliver genome-editing components for Cas9-directed HDR[8], microhomology-mediated end joining[10] and base editing[11] in this mouse model, use of the same delivery method for prime editors should facilitate a comparison of prime editing with the other genome-editing approaches.

To find a pegRNA that could induce efficient prime editing to correct the pathogenic point mutation, we first identified PE2 target sequences near the mutation site, which were located at positions ranging from −38 base pairs (bp) to +41 bp from the mutation site. Because only two target sequences with an NGG protospacer adjacent motif (PAM) were available near the mutation site, we generated PE2 on the basis of SpCas9-NG (Fig. 1b), a variant of Cas9 from *Streptococcus pyogenes* (SpCas9) that has wider PAM

[1]Department of Pharmacology, Yonsei University College of Medicine, Seoul, Republic of Korea. [2]Brain Korea 21 Plus Project for Medical Sciences, Yonsei University College of Medicine, Seoul, Republic of Korea. [3]Department of Anatomy and Cell Biology, Seoul National University College of Medicine, Seoul, Republic of Korea. [4]Fight against Angiogenesis-Related Blindness (FARB) Laboratory, Biomedical Research Institute, Seoul National University Hospital, Seoul, Republic of Korea. [5]Center for Nanomedicine, Institute for Basic Science (IBS), Seoul, Republic of Korea. [6]Graduate Program of Nano Biomedical Engineering (NanoBME), Advanced Science Institute, Yonsei University, Seoul, Republic of Korea. [7]Department and Research Institute of Rehabilitation Medicine, Yonsei University College of Medicine, Seoul, Republic of Korea. [8]Graduate Program of NanoScience and Technology, Yonsei University, Seoul, Republic of Korea. [9]Genome Editing Research Center, Korea Research Institute of Bioscience and Biotechnology (KRIBB), Daejeon, Republic of Korea. [10]Department of Biomedical Sciences, Seoul National University College of Medicine, Seoul, Republic of Korea. [11]Department of Ophthalmology, Seoul National University College of Medicine, Seoul, Republic of Korea. [12]Severance Biomedical Science Institute, Yonsei University College of Medicine, Seoul, Republic of Korea. [13]These authors contributed equally: Hyewon Jang and Dong Hyun Jo. ✉e-mail: steph25@snu.ac.kr; hkim1@yuhs.ac

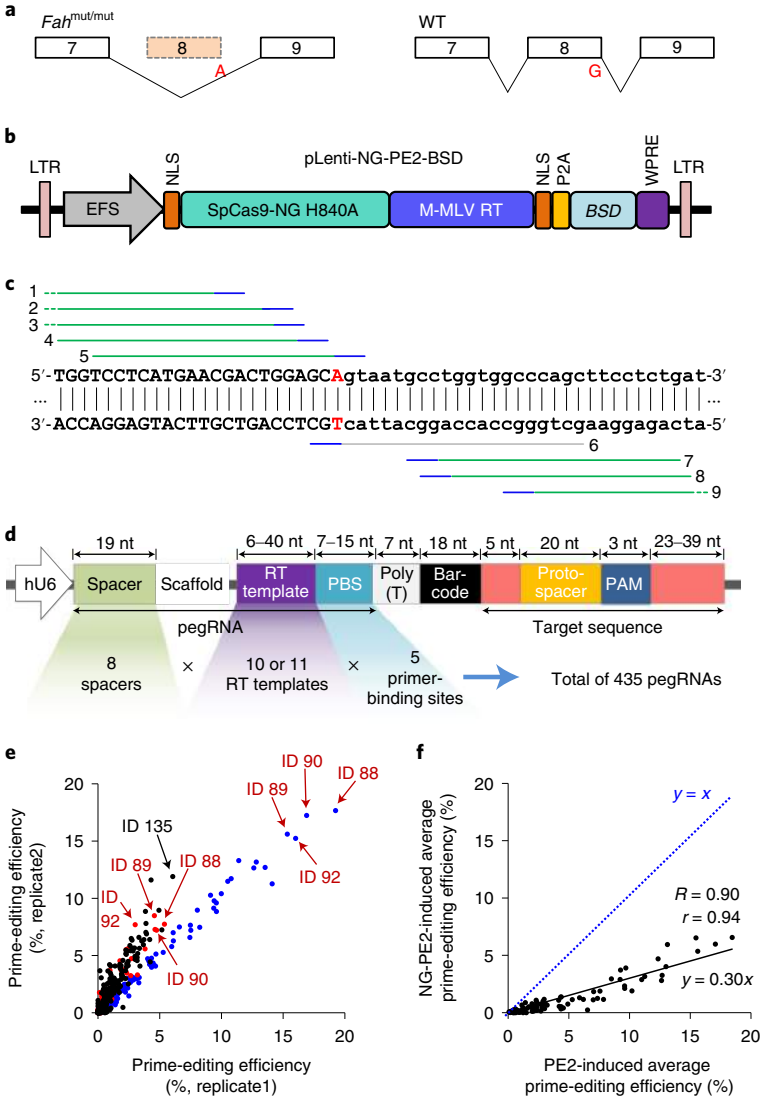

Fig. 1 | A mouse model of tyrosinemia and high-throughput evaluation of pegRNAs. a, Exon 8 skipping in *Fah*$^{mut/mut}$ mice. The G-to-A point mutation (red) at the last nucleotide of exon 8 of the *Fah* gene leads to exon 8 skipping during splicing. **b**, A schematic representation of the plasmid encoding NG-PE2. NG-PE2, a fusion of SpCas9-NG H840A nickase with Moloney murine leukaemia virus reverse transcriptase (M-MLV RT), is expressed from the elongation factor 1α short promoter (EFS). The protein encoded by the blasticidin-resistance gene (*BSD*) is co-expressed as a fusion with PE2, from which it is cleaved by the self-cleaving P2A. LTR, long terminal repeat; NLS, nuclear localization sequence; P2A, porcine teschovirus-1 2A; WPRE, woodchuck hepatitis virus posttranscriptional regulatory element. **c**, SpCas9-NG-based PE2 target sequences for correction of the disease-causing point mutation in *Fah*. The protospacer and PAM of each target sequence are represented by green and blue lines, respectively. The numbers on the left and right indicate the target sequence IDs. Exon and intron sequences are shown in upper and lower case letters, respectively. **d**, A schematic representation of the lentiviral library of pegRNA–target sequence pairs. Each pegRNA is paired with a wide target sequence that includes a protospacer, a PAM and neighbouring sequences. pegRNA expression is driven by the human U6 promoter (hU6). The library included a total of 435 pegRNA–target pairs, with the pegRNAs containing PBSs of five different lengths (7, 9, 11, 13 or 15 nt) and 10 to 11 different RT template lengths (6 to 40 nt). Spacer, guide sequence of pegRNA. **e**, Prime-editing efficiencies in replicates independently transfected with the NG-PE2- or PE2-encoding plasmid. The red and black dots indicate NG-PE2-induced editing using pegRNAs with corresponding target sequences with NGG and NGH PAMs, respectively, whereas the blue dots represent PE2-induced editing using pegRNAs with target sequences with NGG and NGH PAMs. The IDs of pegRNAs that showed high efficiencies using NG-PE2 and PE2 are indicated with red and black arrows. The number of pegRNA and target sequence pairs $n = 339$ for experiments in which NG-PE2 was used (black and red dots) and $n = 339$ for experiments in which PE2 was used (blue dots) (out of 435 pairs, those evaluated in both replicates after filtering out pairs with insufficient read counts or high levels of background editing are shown (Methods)). **f**, Comparison of PE2- and NG-PE2-induced prime-editing efficiencies at target sequences with NGG PAMs. The position where PE2 and NG-PE2-induced efficiencies would be the same is shown using a blue dashed line ($y = x$). The Spearman (R) and Pearson (r) correlation coefficients are shown. $n = 100$ pegRNA and target sequence pairs.

compatibility than SpCas9[12–14]. We identified nine target sequences for SpCas9-NG-based PE2 (hereafter NG-PE2) for the intended editing of the point mutation (Fig. 1c). Given that Cas9 nuclease activity is one of the most important factors determining PE2 efficiency[2], we first calculated the predicted nuclease activity of SpCas9-NG at the nine sites using DeepSpCas9-NG[14]. One of the nine target sequences (target ID 6) showed a very low predicted activity (Supplementary Table 1), so we removed that target sequence from subsequent

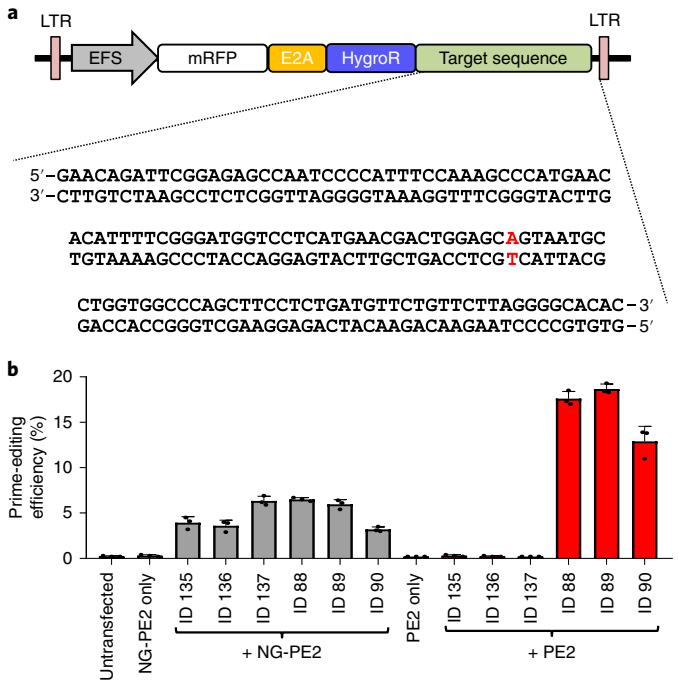

Fig. 2 | Evaluation of PE2 efficiencies using target sequence–containing cells. a, Schematic representation of the lentiviral vector containing the mutant *Fah* target sequence found in *Fah*$^{mut/mut}$ mice. The target sequence is shown; the mutant base pair is shown in red. HEK 293T cells were transduced with this lentiviral vector to generate target sequence–containing cells. mRFP, monomeric red fluorescent protein; E2A, equine rhinitis A virus 2A; HygroR, hygromycin resistance. **b**, Prime-editing efficiencies of six pegRNAs (IDs 88, 89, 90, 135, 136 and 137) in the target sequence–containing cells when combined with NG-PE2 or PE2. Frequencies were measured 5 d after transfection of a pegRNA-encoding plasmid and a PE2- or NG-PE2-encoding plasmid. The ID of the pegRNA used is shown on the *x*-axis. Data are mean ± s.d. $n = 3$ independent transfections.

pegRNA evaluations. For the remaining eight target sequences, we designed pegRNAs containing primer binding sites (PBSs) of five different lengths (7, 9, 11, 13 or 15 nucleotides (nt)) and 10 to 11 different RT template lengths (6 to 40 nt) (Fig. 1d).

To undertake a high-throughput evaluation of the resulting 435 pegRNAs, we generated a lentiviral library containing the 435 pegRNA-encoding sequences paired with the corresponding target sequences[2] (Extended Data Fig. 1). Next, this lentiviral library was transduced into HEK 293T cells to make cell libraries. These cell libraries were then transiently transfected with plasmids encoding NG-PE2. Five days after the transfection, the target sequences were analysed by deep sequencing. The highest prime-editing efficiency (9.0%) was observed with a pegRNA (pegRNA ID 135) that targets a sequence with an NGT PAM (Fig. 1e, Supplementary Table 2). The second (7.9%) and third (6.9%) highest prime-editing efficiencies were also observed with pegRNAs (pegRNA IDs 136 and 137) that target the same sequence targeted by pegRNA ID 135. The fourth and fifth highest prime-editing efficiencies were 6.6% and 6.5%, which were observed with two pegRNAs (pegRNA IDs 88 and 89, respectively; Supplementary Table 2) targeting a common sequence (target sequence ID 2) with an NGG PAM. However, according to DeepSpCas9-NG[14], the predicted SpCas9-NG nuclease activity at the NGT PAM-containing target sequence that corresponds to pegRNA ID 135 was only 17.0, which was substantially lower than 52.4, the SpCas9 nuclease activity predicted by DeepSpCas9[15] at the NGG PAM-containing target sequence (Supplementary Table 2). Thus, we expected that the prime-editing efficiencies of PE2 with pegRNA ID 88 or 89 would be higher than that of NG-PE2 with pegRNA ID 135. To test this expectation, we performed the same high-throughput evaluation experiments using PE2 instead of NG-PE2. As expected, PE2-driven prime-editing efficiencies were substantially higher than those induced by NG-PE2 at target sequences with NGG PAMs (mean and median fold increases were 3.9- and 3.6-fold, respectively; for accuracy of the fold-increase calculation, pegRNAs that showed NG-PE2-induced efficiencies lower than 0.5% were excluded from the calculation) (Fig. 1f). The top four highest prime-editing efficiencies induced by PE2 were 18.5%, 17.1%, 15.6% and 15.5% (obtained using pegRNA IDs 88, 90, 92 and 89, respectively), which were all higher than the highest prime-editing efficiency of 9.0% obtained using NG-PE2 (Fig. 1e).

Evaluation of PE2 efficiencies using target sequence–containing cells. We next tested the three pegRNAs that showed the highest editing efficiencies with NG-PE2 (IDs 135, 136 and 137) and the three pegRNAs associated with an NGG PAM that showed the highest efficiency with NG-PE2 (IDs 88, 89 and 90) by individual evaluations. We generated HEK 293T cells containing the target sequence by transduction of target sequence–containing lentiviral vector (Fig. 2a). The cells were transiently transfected with plasmids encoding NG-PE2 and pegRNA 135, 136 or 137 or plasmids encoding PE2 and pegRNA 88, 89 or 90. Deep sequencing showed that the average PE2-directed prime-editing efficiencies of pegRNAs 88, 89 and 90 were 17.6%, 18.7%, and 12.9%, respectively, which were higher than the NG-PE2-induced prime-editing efficiencies of pegRNAs 135, 136 and 137 (3.9%, 3.6%, and 6.3%, respectively) (Fig. 2b). Thus, we chose pegRNA 89, which showed the highest editing efficiency, for subsequent studies.

PE3 corrects the disease mutation and phenotype in *Fah*$^{mut/mut}$ mice. The initial study of prime editing suggested that the editing efficiency of PE3 and PE3b would generally, albeit not always, be higher than that of PE2 when tested in cultured mammalian cells[1]. Thus, we attempted to use PE3 or PE3b for in vivo genome editing by adding an sgRNA. On the basis of the DeepSpCas9 score[15], we selected a highly active sgRNA (ID 1) that enables PE3 (Supplementary Table 3, Supplementary Fig. 1a).

We next delivered plasmids encoding the selected pegRNA, the sgRNA and PE2 (Supplementary Fig. 1b–d) into 5- to 7-week-old *Fah*$^{mut/mut}$ mice using hydrodynamic injection, after which the mice were treated with NTBC for 7 d (Fig. 3a). After discontinuation of NTBC, all mice that had received PE3 (that is, PE2, pegRNA and sgRNA) survived until the end of the experiment (40 d), whereas all mice injected with phosphate-buffered saline as a negative control showed substantial weight loss and died before 30 d (Fig. 3b). This extended survival and the prevention of weight loss suggest PE3-induced amelioration of the disease phenotype, which is consistent with the results of previous studies involving genome editing in this mouse model[6–8,10,11].

To evaluate whether prime editing rescues exon 8 skipping, at the end of the experimental period (40 d) we conducted PCR with reverse transcription (RT–PCR) using liver mRNA as the template[11] and primers binding exons 5 and 9. A 305-bp PCR amplicon, which indicates exon 8 skipping, was observed for *Fah*$^{mut/mut}$ mice, whereas a single 405-bp PCR amplicon, which indicates that exons 5 to 9 are intact, was seen for wild-type mice (Fig. 3c). All five mice injected with PE3 showed both 305- and 405-bp amplicons, suggesting that exon 8 skipping was rescued in a fraction of hepatocytes. Sequencing of the 405-bp amplicon confirmed that the mutant sequence was corrected at the mRNA level (Fig. 3d). Quantitative RT–PCR (RT–qPCR) revealed that the relative average level of exon 8-containing *Fah* mRNA in PE3-treated *Fah*$^{mut/mut}$ mice was 12% of

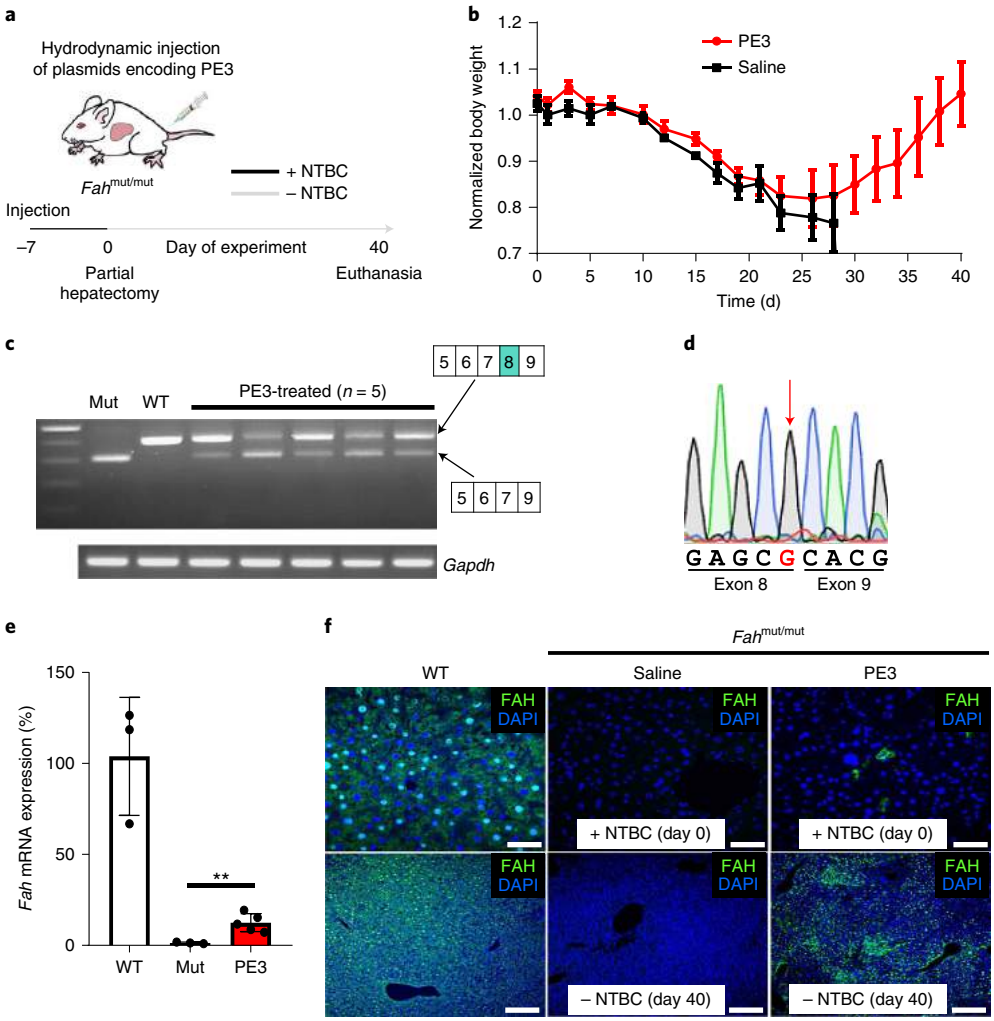

Fig. 3 | PE3 corrects the disease mutation and phenotype in *Fah*$^{mut/mut}$ mice. a, A schematic representation of the experiments. *Fah*$^{mut/mut}$ mice underwent hydrodynamic injection of plasmids encoding PE3 components (that is, PE2, pegRNA and sgRNA) and were kept on water containing NTBC for 7 d. The day on which NTBC was withdrawn is defined as day 0. On day 0, a partial hepatectomy was performed to collect liver tissue. At 40 d, the PE3-treated mice were euthanized and analysed. **b**, Body weight of *Fah*$^{mut/mut}$ mice injected with PE3 or phosphate-buffered saline (saline control). Body weights were normalized to the pre-injection weight. $n = 5$ (PE3) and $n = 3$ (saline) mice. Data are mean ± s.e.m. **c**, Representative RT–PCR using RNA isolated from the liver at 40 d. The primers hybridized to sequences in exons 5 and 9. The wild-type (WT) *Fah*$^{+/+}$ amplicon (top band) is 405 bp in length and the mutant (Mut) amplicon (which lacks exon 8) (lower band) is 305 bp. *Gapdh* was used as a control. **d**, Representative results from Sanger sequencing of the 405-bp RT–PCR band from the PE3-treated mice shown in **c**. The red arrow indicates the corrected G nucleotide, which is shown in red. **e**, Wild-type *Fah* mRNA in the liver was quantified by RT–qPCR using primers that hybridize to sequences in exons 8 and 9. WT, wild-type mice; Mut, *Fah*$^{mut/mut}$ mice; PE3, *Fah*$^{mut/mut}$ mice injected with plasmids encoding PE3 components. Data are mean ± s.d. $n = 3$ (WT), 3 (Mut) and 5 (PE3) mice. $^{**}P = 0.0093$. **f**, Immunofluorescence staining of FAH protein. Saline, phosphate-buffered saline control. Scale bars: 50 μm (top row), 200 μm (bottom row).

that in wild-type mice, whereas such mRNA was not detectable in control *Fah*$^{mut/mut}$ mice (Fig. 3e), corroborating that PE3 corrected the exon 8 skipping mutation.

We next quantified the frequency of FAH$^+$ cells in the livers of PE3-treated mice. Immunofluorescence staining showed that FAH$^+$ cells were present at an average frequency of 0.07% (range, 0.01% to 0.12%) at day 0 (the day NTBC was discontinued) and at an average frequency of 61% (range, 45% to 75%) at day 40 (Fig. 3f and Supplementary Fig. 2). Deep sequencing of liver DNA revealed that the intended edit was not detectable at day 0 (data not shown), which is in line with a previous study of HDR-based genome editing using this mouse model[8]. The intended edit was present at an average frequency of 11.5% (range, 6.7% to 18%) at day 40 (Fig. 4a). The reason that the frequency of FAH$^+$ cells is higher than the frequency of editing at the DNA level would be because the majority of hepatocytes are polyploid[16] and because nonparenchymal cell DNA is mixed with that of hepatocytes; similar results were observed in the previous genome-editing studies using this mouse model[8,11]. The observed editing efficiencies are comparable to those obtained with previous approaches using HDR (9.3% at 33 d after the delivery of genome-editing components and 30 d after NTBC withdrawal)[8], microhomology-mediated end joining (5.2% at 37 d after the delivery of genome-editing components and 30 d after NTBC withdrawal)[10] and base editing (9.5% at 38 d after the delivery of genome-editing components and 32 d after NTBC withdrawal)[11] in this mouse model when the genome-editing components were delivered using hydrodynamic injections, although direct comparisons are difficult due to the differences in the time points at which the editing efficiencies were analysed and at which NTBC was discontinued.

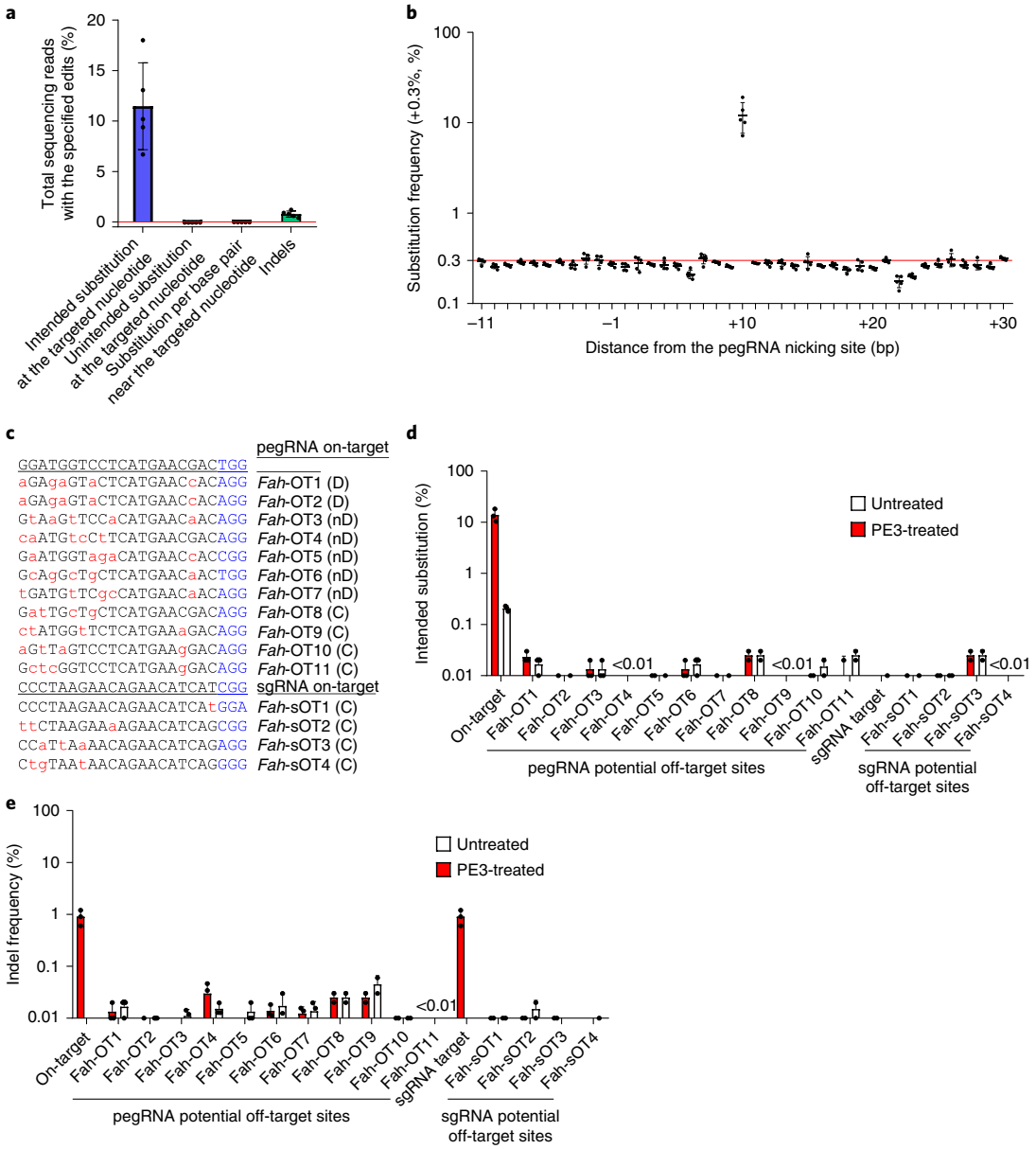

Fig. 4 | PE3 corrects the disease-causing mutation in a highly precise manner. a, Frequencies of intended and unintended edits in the livers of PE3-treated mice. The frequencies were normalized by subtracting the average frequency of such editing in the control group injected with phosphate-buffered saline to exclude errors originating from PCR amplification and sequencing. Substitutions near the targeted nucleotide were evaluated over a 40-bp range centred on the targeted nucleotide. Indels were assessed over a 136-bp range centred on the pegRNA nicking site. The red horizontal line represents the point where the normalized frequency is zero. Data are mean ± s.d. $n = 5$ mice. **b**, Substitution frequencies at positions ranging from −20 bp to +20 bp of the target nucleotide in PE3-treated mice. The frequencies were normalized by subtracting the average edit frequencies in the control group injected with phosphate-buffered saline to exclude errors originating from PCR amplification and sequencing. The red horizontal line represents the location where the normalized frequency is zero (to show the values on a logarithmic scale, 0.3% was added to every value on the *y* axis). Positions are numbered from the pegRNA nicking site. The targeted position is at +10. Data are mean ± s.d. $n = 5$ mice. **c**, Potential off-target sites experimentally captured by Digenome-seq (D) and nDigenome-seq (nD) or computationally predicted by CRISPOR (C). Nucleotides in red indicate mismatched sequences, and nucleotides in blue represent PAM sequences. **d**,**e**, Frequencies of the intended substitution (**d**) and indels (**e**) at the 11 potential off-target sites for the used pegRNA (ID 89) (OT1–OT11) and at the four potential off-target sites for the used sgRNA (sOT1–sOT4) in PE3-treated liver tissues. Genomic DNA isolated from the livers of *Fah*$^{mut/mut}$ mice without PE3 treatment was used as the negative control (untreated). $n = 2$ or 3 mice.

PE3 corrects the disease-causing mutation in a highly precise manner. We next determined whether PE3 induced any unintended editing including insertion–deletions (indels) in or near the target sequence in the mouse liver. Deep sequencing revealed that unintended substitutions at or near the targeted nucleotide were not detected in any of the mice and that the level of indels ranged from only 0.4% to 1.2% (average, 0.78%) (Fig. 4a,b). In the case of the Cas9-directed HDR approach, the frequency of indels observed at the target site was 26%, which is 33-fold higher than the level induced by PE3 in this study. When adenosine base editor was used, the frequency of unintended substitutions observed near the target nucleotide[11] was 1.9%. Thus, these data suggest that prime

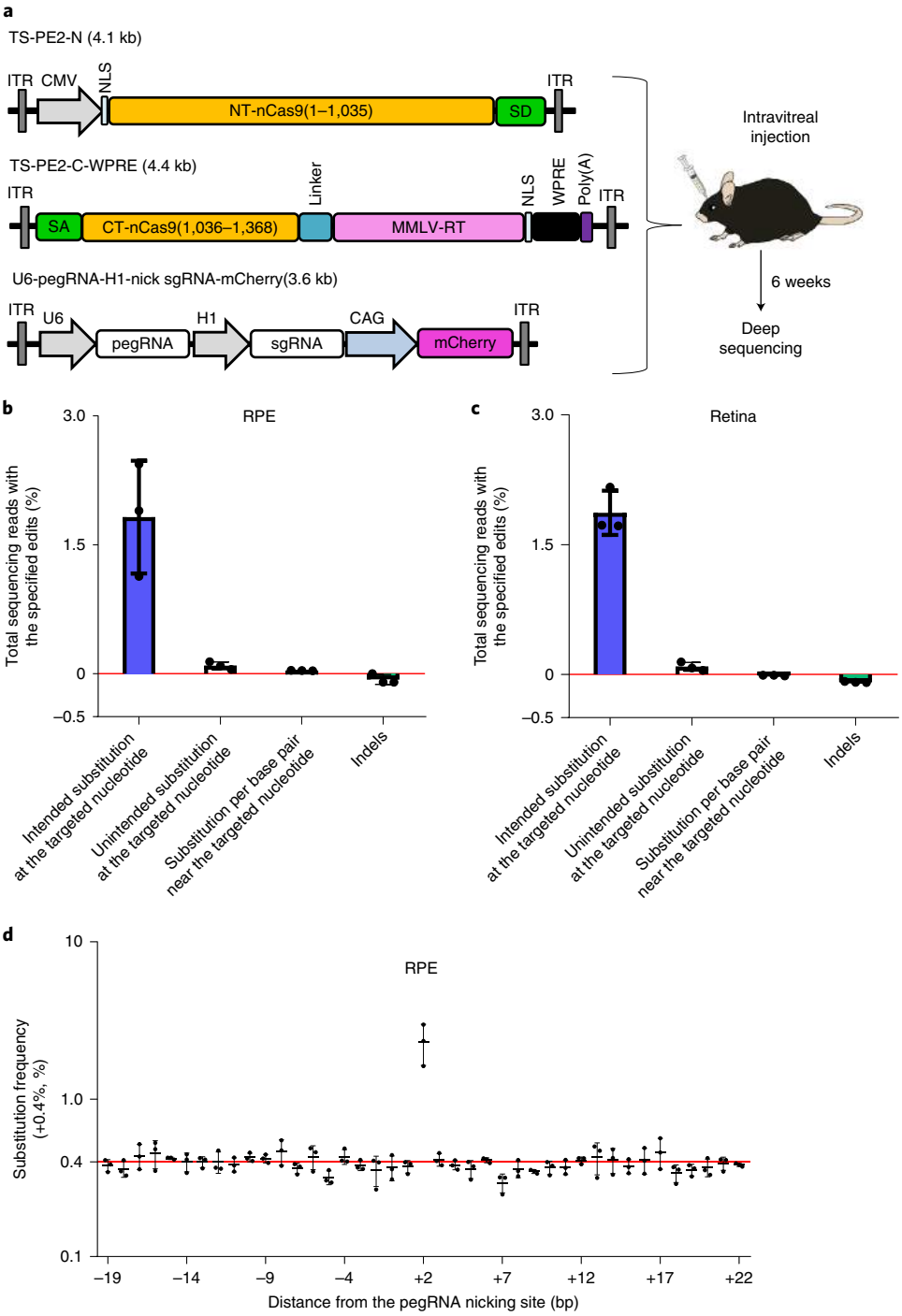

Fig. 5 | AAV-mediated prime editing in the retina and RPE of wild-type mice. a, Schematic representation of experiments together with maps of the AAV vectors used. The lengths of the sequences between the two inverted terminal repeats (ITRs) in each vector are shown in parentheses. Two *trans*-splicing PE2-expressing AAVs (TS-PE2-N and TS-PE2-C-WPRE) were delivered together with an AAV expressing pegRNA and sgRNA into the retina and RPE via intravitreal injection. The retina and RPE cells were collected for deep sequencing six weeks after the injection. NT-nCas9, N-terminal region of SpCas9 H840A nickase; SD, splicing donor; SA, splicing acceptor; CT-nCas9, C-terminal region of SpCas9 H840A nickase. **b**,**c**, Frequencies of intended and unintended edits in the RPE (**b**) and retina (**c**) of PE3-treated mice. The frequencies were normalized by subtracting the average frequencies of such edits in the negative control group that were not injected with PE3 to exclude errors originating from PCR amplification and sequencing. Substitutions near the targeted nucleotide were evaluated over a 40-bp range centred on the targeted nucleotide. Indels were measured over a 136-bp range centred on the pegRNA nicking site. The red horizontal line represents the location where the normalized frequency is zero. Data are mean ± s.d. $n = 3$ mice. **d**, Substitution frequencies at positions ranging from −20 bp to +20 bp of the target nucleotide in the RPE treated with PE3. The frequencies were normalized by subtracting the background substitution frequencies in controls that were not treated with PE3. The red horizontal line represents the location where the normalized frequency is zero (to show the values on a logarithmic scale, 0.4% was added to every value on the *y* axis). Positions are numbered from the pegRNA nicking site. The targeted position is at +2. Data are mean ± s.d. $n = 3$ mice.

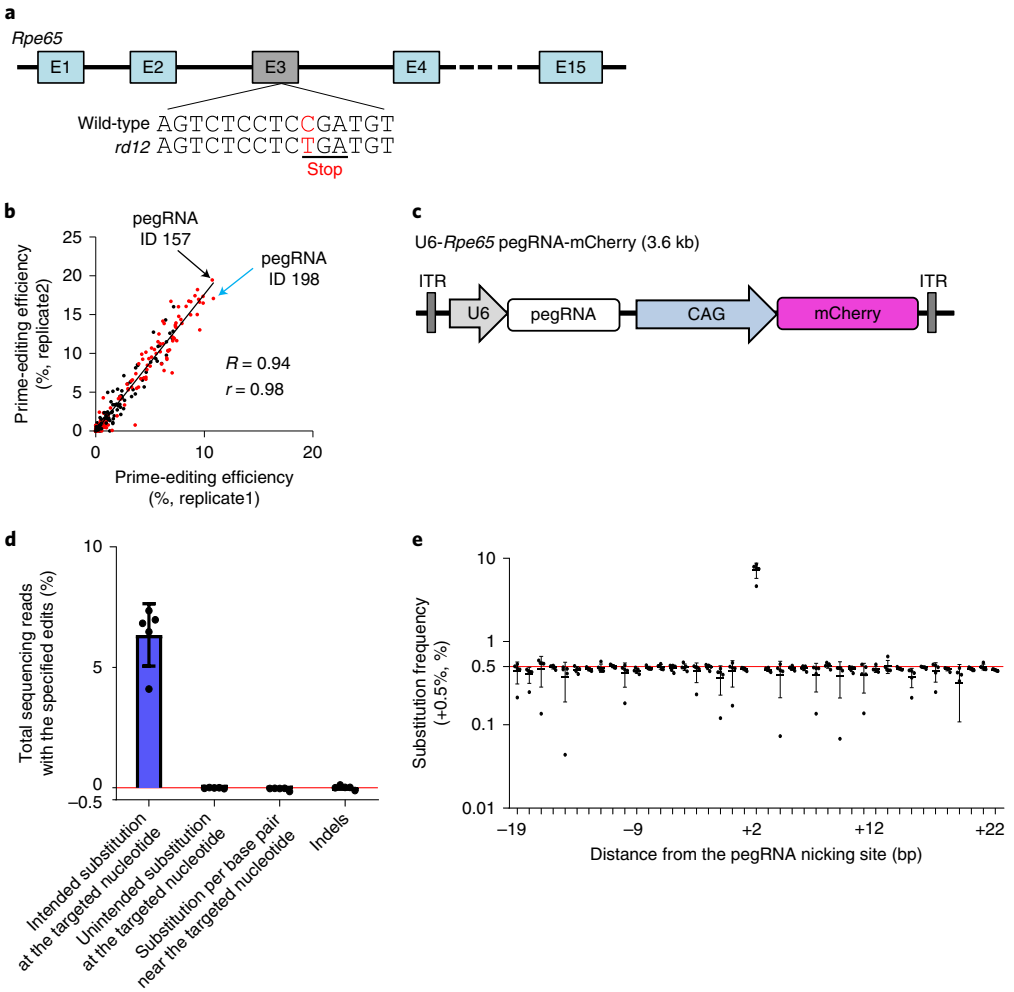

Fig. 6 | Identification of efficient pegRNAs for the correction of the LCA-causing mutation in *rd12* mice, followed by subretinal injection of AAV-PE2 to correct the mutation in vivo. a, The *rd12* mouse model has a homozygous C-to-T nonsense mutation (red) in exon 3 (E3) of the *Rpe65* gene, leading to a premature stop codon (underlined). **b**, The correlation between prime-editing efficiencies in replicates independently transfected with NG-PE2-encoding plasmids. Red and black dots indicate pegRNAs with corresponding target sequences with NGG and NGH PAMs, respectively. The blue arrow indicates the pegRNA selected for subsequent experiments. The Spearman (*R*) and Pearson (*r*) correlation coefficients and trend line are shown. $n = 309$ pegRNA-target sequence pairs. **c**, A vector map of an AAV vector encoding a pegRNA and mCherry. **d**, Frequencies of intended and unintended edits in the RPE of AAV-PE2-treated *rd12* mice. The frequencies were normalized by subtracting the average frequency of such editing in the control group without AAV-PE2 injection to exclude errors originating from PCR amplification and sequencing. Substitutions near the targeted nucleotide were evaluated over a 40-bp range centred on the target nucleotide. Indels were measured over a 60-bp range centred on the pegRNA nicking site. The red horizontal line represents the location where the normalized frequency is zero. Data are mean ± s.d. $n = 5$ mice. **e**, Substitution frequencies at positions ranging from −20 bp to +20 bp from the target nucleotide, in the RPE of PE2-treated *rd12* mice. The frequencies were normalized by subtracting the average edit frequencies in the RPE of *rd12* mice without PE2 treatment to exclude errors originating from PCR amplification and sequencing. The red horizontal line represents the location where the normalized frequency is zero (to show the values on a logarithmic scale, 0.5% was added to every value on the *y* axis). Positions are numbered from the pegRNA nicking site. The targeted position is at +2. Data are mean ± s.d. $n = 5$ mice.

editing can be more precise than the other approaches in mouse somatic cells.

To quantify the off-target effects of PE3, we identified 11 potential off-target sites of the pegRNA using Digenome-seq and nDigenome-seq—unbiased experimental methods to find potential off-target sites for a pegRNA[17,18], and CRISPOR[19]—a computational method, as well as 4 potential off-target sites of the used sgRNA using CRISPOR[19] (Supplementary Table 4). Given that prime editor is based on H840A Cas9 nickase, nDigenome-seq should be sufficient as an unbiased experimental method for identifying potential off-target sites. However, given that most studies—including the initial study of prime editing—used Cas9 nuclease to experimentally[1,20] or computationally[5,21] identify potential off-target sites of prime editing, using both Digenome-seq and nDigenome-seq would be a more inclusive approach, which could lead to more thorough analysis of potential off-target sites and enable possible comparisons with results from the other studies based on Cas9 nuclease. Deep sequencing revealed no off-target effects, including intended substitutions or indels, at any of the 15 sites (Fig. 4c–e). This highly specific editing by PE3 is in line with results showing that off-target effects were not detectable when PE3 was used in mouse embryos[5] or human organoids[3] and is also compatible with the low frequency of off-target effects of PE3 in cultured mammalian cells[1,18].

PE2 corrects the disease mutation and phenotype in *Fah*$^{mut/mut}$ mice. We also performed similar experiments using PE2, which

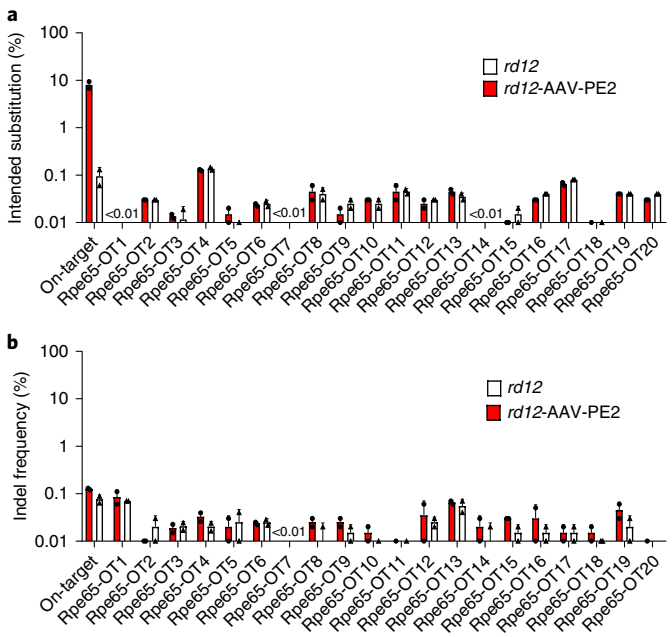

Fig. 7 | Subretinal injection of AAV-PE2 corrects the disease-causing mutation without any detectable off-target effects in *rd12* mice. **a**,**b**, Frequencies of intended edits (**a**) and indels (**b**) at the predicted off-target sites for the pegRNA (ID 198) in the RPE of PE2-treated *rd12* mice. Genomic DNA isolated from the RPE of *rd12* mice without PE2 treatment was used as the negative control (*rd12*). Data are mean ± s.d. $n = 2$ mice.

does not require an sgRNA, instead of PE3 (Extended Data Fig. 2a). *Fah*$^{mut/mut}$ mice treated with PE2 (not NG-PE2) and the pegRNA used for the PE3 experiments described above survived until the end of the experiment (60 d after the initial NTBC withdrawal), whereas the control *Fah*$^{mut/mut}$ mice all died within 30 d (Extended Data Fig. 2b). RT–qPCR showed that the expression level of *Fah* mRNA containing intact exon 8 in PE2-treated mutant mice was on average 6.9% of that in wild-type mice, but that the expression in untreated mutants was undetectable (Extended Data Fig. 2c). Immunofluorescence staining showed that an average of 33% of liver cells from PE2-treated mutant mice were FAH$^+$ at 60 d (Extended Data Fig. 2d).

PE2 corrects the mutation without any detectable unintended substitutions, indels, bystander effects or off-target effects. We analysed genomic DNA isolated from the PE2-injected mice. When the mice were treated with NTBC up to day 0 (7 d after PE2 injection) without partial hepatectomy, the intended editing was not detected (data not shown). When analysed by deep sequencing at the end of the experiments (60 d after the initial NTBC withdrawal), we found that the intended edit was present in an average of 4.0% (range, 2.4% to 5.9%) of the total sequencing reads (Supplementary Fig. 3a). No unintended edits, including indels, unintended substitutions at the targeted nucleotide or bystander-nucleotide edits, were detectable (Supplementary Fig. 3a,b). Furthermore, no off-target effects, including substitution mutations or indels, were detected when we evaluated the 11 potential off-target sites of the pegRNA using Digenome-seq[17], nDigenome-seq[18] and CRISPOR[19] (Supplementary Fig. 3c,d and Supplementary Table 4). Together, these results suggest that PE2-mediated prime editing in mice can correct the disease-causing mutation in a highly precise and specific manner, which could not have been achieved using other previously used genome-editing approaches based on either a CRISPR nuclease or a base editor.

AAV-mediated prime editing in the retina and retinal pigment epithelium of wild-type mice. We next investigated whether prime editing could be achieved in a different adult tissue using a different delivery method. Given that there are several genetic retinal diseases that could potentially be treated using therapeutic genome editing[22], we chose to test in vivo prime editing in the retina of adult mice. We also chose adeno-associated virus (AAV) for the delivery of PE2-, pegRNA- and sgRNA-encoding sequences, because AAV has been used to efficiently deliver sequences encoding other genome-editing tools including engineered nucleases and base editors. Given that the coding sequence of PE2 is 6,273 bp long, which is longer than the cargo size limit of AAV, we used the trans-splicing AAV (tsAAV) vector[23–25] (serotype 8) (Fig. 5a). As a proof-of-concept study of prime editing in the retina, we chose to target the *Atp7b* gene, because editing this gene is not expected to affect the viability or function of retinal cells. We designed four pegRNAs that would induce a G-to-A substitution and chose the one associated with the highest activity (8.3%) in cultured neuro2A cells (Supplementary Fig. 4a,b). An sgRNA that was predicted to be highly active was selected using DeepSpCas9[15] (Supplementary Fig. 4a and Supplementary Table 5).

AAV-mediated prime editing in the retina and RPE did not induce any detectable unintended substitutions, indels, bystander effects or off-target effects. We delivered two tsAAV vectors, one encoding the N-terminal half of PE2 and the other encoding the C-terminal half, together with an AAV vector encoding the *Atp7b*-targeting pegRNA and sgRNA, into the mouse retina and retinal pigment epithelium (RPE) using intravitreal injection. Six weeks after the injection, the mice were euthanized and the RPE and retina were collected and analysed (Fig. 5a). Deep sequencing showed that the average editing efficiencies were 1.82% and 1.87% in the RPE and retina, respectively, without detectable indels or unintended substitutions at or nearby the targeted nucleotide (Fig. 5b–d and Supplementary Figs. 5 and 6). These data suggest that AAV-mediated PE3 delivery can induce precise genome editing in the retina and RPE of adult mice. Given that a frequency of even 1.17% of the desired edit can lead to a substantial improvement in retinal function in a mouse model of a human genetic eye disease[26], this level of PE3-induced genome editing could be useful for therapeutic genome editing.

We found 11 potential off-target sites of the used pegRNA using Digenome-seq, nDigenome-seq[18] and CRISPOR[19], and four potential off-target sites of the sgRNA using CRISPOR[19] (Supplementary Fig. 7a and Supplementary Table 4). Deep sequencing at those 15 sites revealed no detectable off-target substitutions or indels (Supplementary Fig. 7b,c), corroborating that prime editing is highly specific.

Identification of pegRNAs for in vivo prime editing in a genetic eye disease model. We next investigated whether prime editing could be achieved in another disease model. Leber congenital amaurosis (LCA) encompasses a group of monogenic genetic eye diseases involving retinal degeneration that causes severe early-onset visual deterioration[27,28]. So far, mutations in at least 18 genes have been reported to be associated with LCA. One representative gene, *RPE65*, encodes an isomerohydrolase that produces 11-*cis* retinal, which is essential in the visual cycle[27,29]. Several therapeutic approaches have been tested to rescue the pathology of LCA. Subretinal injection of AAV encoding wild-type RPE65 improved visual function in human patients[30]. However, the possibility that the exogenous transgene might be silenced after a long period of time cannot be ruled out[31,32]. CRISPR–Cas9 nuclease and antisense oligonucleotides have been used to bypass a splicing defect-inducing mutation in *CEP290*, another representative LCA-causing gene, in primates and human patients[33,34]. However, the antisense-oligonucleotide

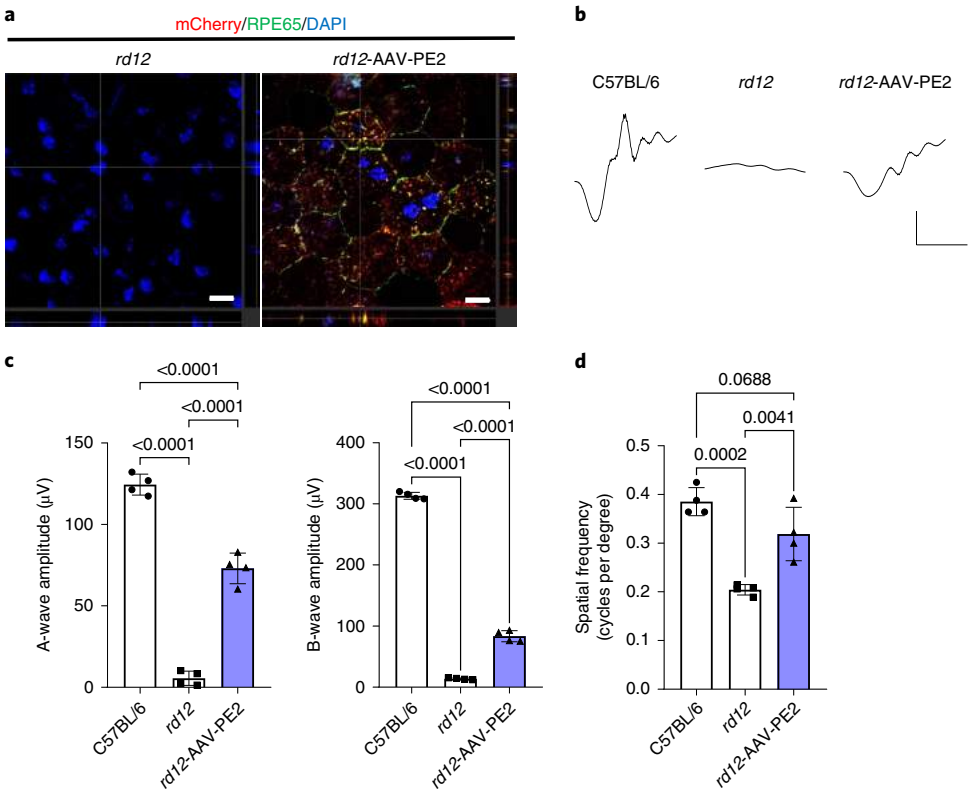

Fig. 8 | Restoration of RPE65 expression and improvement of visual function in *rd12* mice after subretinal injection of AAVs encoding PE2 and the pegRNA (AAV-PE2). a, Representative confocal photomicrographs showing RPE65 protein expression in RPE cells in *rd12* mice 6 weeks after subretinal injection of AAV-PE2. The uninjected negative control is shown on the left. Scale bars, 10 μm. **b**, Representative waveforms of dark-adapted ERG responses at 0 dB in wild-type (C57BL/6), uninjected control (*rd12*), and *rd12* mice injected with PE2-expressing AAV (*rd12*-AAV-PE2). Scale bars, 30 ms (*x*-axis) and 50 μV (*y*-axis). **c**, Amplitudes of a-waves (left) and b-waves (right) of ERG reponses of C57BL/6 and *rd12* mice. Data are mean ± s.d. $n = 4$ mice. *P*-values from one-way ANOVA with post hoc Tukey's multiple comparisons tests are shown. **d**, Optomotor response test results. Data are mean ± s.d. $n = 4$ mice. *P*-values from one-way ANOVA with post hoc Tukey's multiple comparisons tests are shown.

approach required repeated injections and the Cas9-based approach that involved bypassing a splicing defect can induce unintended indels and is restricted to mutations that cause splicing defects. A more promising approach would be to correct the mutation, generating the wild-type sequence. As potential methods for correcting an LCA-associated mutation, CRISPR–Cas9-directed HDR[26] and adenine base editing[35,36] have been evaluated in the *rd12* mouse model of *RPE65*-related LCA. However, these approaches resulted in limited precision, causing substantial indel frequencies[26] or unintended bystander editing[35,36]. A method for the precise correction of the disease mutation in eyes would be a promising option for treating LCA and other genetic diseases.

To determine whether delivery of a PE using a clinically applicable method could both precisely correct the causal mutation and rescue the phenotype of a genetic eye disease, we used *rd12* mice, which possess a nonsense mutation caused by a C-to-T transition at position 130 in exon 3 of the *Rpe65* gene (p.R44X)[37] (Fig. 6a). To find an efficient pegRNA for prime editing of this point mutation, we identified possible target sequences with NGN PAMs at positions ranging from −52 bp to +59 bp away from the mutation site (Supplementary Fig. 8a). Among the resulting ten target sequences, six had NGG PAMs and four had NGH PAMs. We designed a total of 561 pegRNAs containing 5 to 6 different lengths (7, 9, 11, 13, 15 or 17 nt) of PBSs and 9 to 17 different lengths (6 to 62 nt) of RT templates for the 10 target sequences (Supplementary Fig. 8b and Supplementary Table 6). To evaluate the efficiencies of these pegRNAs, we constructed a lentiviral library containing the 561 pairs of pegRNA-encoding and corresponding target sequences as similarly performed above (Supplementary Fig. 8b). HEK 293T cells were sequentially transduced with the lentiviral library and transfected with plasmids encoding NG-PE2 as conducted for the *Fah*$^{mut/mut}$ model. Deep sequencing of the treated cells showed that the highest (15%) and second-highest (14%) average prime-editing efficiencies were achieved with two pegRNAs (pegRNA IDs 157 and 198, respectively) that recognized the same target sequence with an NGG PAM (ID 5) and that had the same PBS length (9 nt) (Fig. 6b and Supplementary Table 6). The only difference between the two pegRNAs was the RT template length (13 and 14 nt in IDs 157 and 198, respectively). Because the first replicate study showed that pegRNA ID 198 had the highest efficiency, we chose this pegRNA for the subsequent quick application of prime editing in *rd12* mice; however, the average of results from two replicates later showed that pegRNA ID 157 had the highest efficiency. In addition, we used PE2 instead of NG-PE2 because SpCas9 showed higher activities than SpCas9-NG at target sequences with an NGG PAM[14] and PE2 showed higher general activities than NG-PE2 at targets with an NGG PAM[38].

PE2 precisely corrects the disease mutation in a mouse model of LCA. To investigate the therapeutic potential of prime editing in *rd12* mice, we used the AAV system with serotype 2 to express PE2 (Fig. 5a) and the selected pegRNA (pegRNA ID 198) (Fig. 6c). We injected this system, named AAV-PE2, subretinally into 3-week-old *rd12* mice. When the mice were analysed 6 weeks after the injection, we observed that on average, 23% (range, 17% to 30%) of the whole RPE area in the *rd12* mice was mCherry-positive (Supplementary Fig. 9), reflecting the delivery efficiency of AAV-PE2[39].

Deep sequencing of genomic DNA isolated from the RPE tissue showed an average prime-editing efficiency of 6.4% (range, 4.1% to 7.4%) (Fig. 6d). Given that AAV-PE2 was delivered to only 23% of the RPE, the editing efficiency in regions that were exposed to prime-editing components can be estimated to be, on average, 28%. Importantly, no unintended edits, substitutions or indels were detectable near the mutation site (Fig. 6d,e), suggesting highly precise genome editing in this disease model using a clinically applicable delivery approach. In our previous attempt using a CRISPR nuclease-mediated HDR approach in the same mouse model[26], the correction efficiency was 1.2% ± 0.3% with an indel frequency of 17% ± 8%. Lentivirus and AAV-mediated delivery of adenine base editors resulted in editing efficiencies of 16% ± 3% and 11% ± 7%, respectively, with substantial (up to 17% (lentivirus) and 7.7% ± 5% (AAV)) frequencies of bystander edits within the base editor editing windows[35,36]. We cannot rule out the possibility that such unintended edits could cause adverse effects, including unwanted immune responses against the protein variants encoded by genes affected by the unintended editing.

When we evaluated off-target effects at 20 potential off-target sites identified using Digenome-seq[17], nDigenome-seq[18] and Cas-OFFinder[40] (Supplementary Fig. 10 and Supplementary Table 4), neither indels nor intended editing were observed (Fig. 7). This lack of off-target effects is in line with a failure to find off-target effects of prime editing in mouse embryos[5] and human organoids[3] even when PE3 was used (off-target effects of PE3 would be, at a minimum, a combination of the off-target effects of PE2 and those of the sgRNA). Together, our results show that subretinal injection of AAV-PE2 induced almost perfectly precise genome editing without bystander editing, generation of indels or off-target effects at the genomic DNA level in the mouse RPE.

In vivo prime editing improves visual function in the mouse model of LCA. We next tested whether this highly precise and specific genome editing would lead to functional correction of the disease. Immunofluorescence staining showed a distinct membranous and cytoplasmic expression of the RPE65 protein in RPE tissue from *rd12* mice treated with AAV-PE2, but not in tissue from untreated control *rd12* mice, at 6 weeks after the subretinal injection (Fig. 8a). As previously reported[26,37], electroretinography (ERG) revealed a lack of dark-adapted light-induced electrical responses in control *rd12* mice. However, AAV-PE2 treatment rescued dark-adapted ERG responses (Fig. 8b). Amplitudes of scotopic a- and b-waves from AAV-PE2-treated *rd12* mice were on average 59% (range, 48% to 67%) and 27% (range, 24% to 30%), respectively, of those of wild-type C57BL/6 mice (Fig. 8c). Compatible with these results, spatial thresholds to virtual rotating stimuli were increased in AAV-PE2-treated *rd12* mice on optomotor response measurements (Fig. 8d). Together, these results show that AAV-PE2-mediated prime editing in mouse RPE substantially improved visual function in *rd12* mice.

AAV-PE2 using the most efficient pegRNA also rescues the genotype and phenotype of LCA. We also conducted the same experiments using pegRNA ID 157, which showed the highest average prime-editing efficiency in the high-throughput evaluation experiments. We observed slightly higher or similar prime-editing efficiencies (an average of 7.7%; range, 4.7% to 16%) (Extended Data Fig. 3a) than when we used pegRNA ID 198, which is in line with the result that pegRNA ID 157 showed slightly higher efficiency than pegRNA ID 198. Similar to the results using pegRNA ID 198, experiments using pegRNA ID 157 did not show unintended editing near the target sequence (Extended Data Fig. 3b). Furthermore, the levels of functional improvements caused by AAV-PE2 using pegRNA ID 157 were overall comparable to those using pegRNA ID 198—ERG showed that AAV-PE2 using pegRNA ID 157 also rescued dark-adapted ERG responses (Extended Data Fig. 3c). Amplitudes of scotopic a- and b-waves from AAV-PE2-treated *rd12* mice were on average 34% (range, 25% to 49%) and 36% (range, 32% to 41%), respectively, of those of wild-type C57BL/6 mice (Extended Data Fig. 3d) and spatial thresholds to virtual rotating stimuli were also increased in AAV-PE2-treated *rd12* mice (Extended Data Fig. 3e). These results corroborate that AAV-PE-induced prime editing can precisely correct the genotype and phenotype of a mouse model of LCA.

Discussion

Our results demonstrate that prime editing can generate intended edits in a highly precise manner in the liver and eye in mouse models of genetic diseases when components are delivered using hydrodynamic injection and AAV-mediated methods, respectively. We also showed that replacing the SpCas9 domain of PE2 with a variant that recognizes a different set of PAMs, such as SpCas9-NG, can expand the list of target sequences for prime editors.

Cells containing disease-causing mutations are often not readily available, which makes it difficult to evaluate the efficiencies of genome-editing tools including prime editors at the mutant target sequence. Furthermore, hundreds or thousands of pegRNAs can be designed to induce an intended edit at a target sequence. Although previously reported rules for designing optimal pegRNAs and computational models that predict pegRNA activities can help narrow down the list of optimal pegRNAs[2], the most thorough and definitive method for identifying the optimal pegRNA would be to evaluate all possible pegRNAs or all pegRNAs suggested by the rules and computational models. For clinical applications of prime editing, the most efficient pegRNAs corresponding to the mutations found in patients would need to be identified. Determination of pegRNA activities using lentiviral libraries of paired pegRNA and target sequences as we describe above would be useful, especially when mutant sequence-containing cell lines are not available or when a large number of pegRNAs are evaluated.

The accuracy of high-throughput evaluations will be increased by using a large number of cells relative to the number of analysed pegRNAs (high coverage), homogenous delivery of prime-editing components and high sequencing read depth per pegRNA. To identify the pegRNA that will work best for a specific application, we recommend the selection of several top-ranking pegRNAs from the high-throughput evaluations and the subsequent individual evaluation of their activities at endogenous loci.

When we compared PE2- and PE3-based correction of the disease-causing mutation in *Fah*$^{mut/mut}$ mice using hydrodynamic injections with those based on the hydrodynamic injections of Cas9 nuclease[8,10] or adenosine base editor[8], the efficiencies were overall comparable, although exact comparisons are difficult, at least in part, due to differences in the time points used for analysis (Supplementary Fig. 11 and Supplementary Table 7). However, the most notable difference is the precision of the editing. Cas9 nuclease induced a substantial frequency of indels (26%) at the target sites and a detectable, albeit lower than 0.3%, frequency of indels at off-target sites[8], whereas adenosine base editor induced considerable bystander effects (1.9%). However, PE3, but not PE2, induced only a low level of indels (on average 0.78%) and bystander or off-target effects were not observed for either PE2 or PE3, although we cannot rule out the possibility of off-target effects that could be identified using more advanced methods that might be developed in the future. The level of precision in genome editing that we observed for PE2 in particular has, to our knowledge, not been achieved using any of the previous methods of genome editing in this mouse model. This precise genome editing is different from results in a recent report[5], in which relatively high levels of PE3-induced unintended substitutions in mouse embryos were described. Differences in the analysis method (we used uninjected negative controls, which allowed us to

subtract background errors originating from sequencing and PCR, whereas this previous study did not use negative controls), target sequences, host animals (adult mice versus embryos) and delivery methods (AAV-mediated delivery versus direct injection of RNAs) might be reasons for the differences in the precision of editing.

The initial PE2- and PE3-induced editing efficiencies, before NTBC withdrawal from *Fah*$^{mut/mut}$ mice, were under the detection limit. Although these low initial editing efficiencies functionally rescued the mice owing to the selective expansion of gene-corrected cells in this model of tyrosinemia, these efficiencies would not be sufficient to obtain satisfactory therapeutic effects in other liver diseases in which gene-corrected cells do not selectively expand. When we delivered PE2 and PE3 using the AAV vector into *Fah*$^{mut/mut}$ mice, the initial editing efficiencies before NTBC withdrawal, measured at the DNA level by deep sequencing, were also below the detection limit (data not shown). Thus, further optimization of the methods for prime-editor delivery could be required for the application of prime editing in human patients with liver diseases, especially for diseases in which the gene-edited cells do not selectively expand.

Here we have shown that highly precise and specific genome editing induced by the delivery of PE2 using a clinically applicable delivery approach (that is, AAV) effectively rescued the visual function of *rd12* mice. It has recently been reported that AAV-mediated delivery of split-intein PE3 induced correction of a pathogenic gene at efficiencies of 0.6% (2 weeks after injection), 2.3% (6 weeks after injection) and 3.1% (10 weeks after injection) in the liver of an α-1 antitrypsin deficiency mouse model[41]. However, this approach induced unintended indels (about 22% of all edited alleles) and, more importantly, did not achieve functional correction. We estimate that the editing efficiency in our experiment was, on average, around 28% or 33% in the AAV-PE2-transduced region. In human patients, ophthalmologists can inject AAV-PE2 near the macula, to augment the editing efficiency in the cells at and near the macula, which is responsible for the major portion of our vision[26,30]. Given that subretinal injection of AAV has been successfully used in clinical trials[30–32], our study will lay a foundation for clinical translation of prime editing for LCA. Furthermore, given that AAV has been used as a delivery method for genetic diseases in organs other than the eyes[42,43], we envision that AAV-mediated delivery of PE2 could be used to treat patients with genetic diseases that affect other organs.

This high precision of prime editing in somatic cells of mice raises the possibility that prime editing could be used for genome editing in human patients. We envision that in vivo prime editing, together with previously reported base editing and engineered nuclease-based approaches, will be a promising tactic for genome-editing therapy for genetic diseases.

Methods

Construction of plasmid vectors. To prepare pLenti-NG-PE2-BSD, the Lenti_Split-BE4-N-Blast plasmid[44] was digested with restriction enzymes AgeI and BamHI (New England Biolabs (NEB)) and a MEGAquick-spin total fragment DNA purification kit (iNtRON Biotechnology) was used to gel purify the linearized plasmid. Fragments of PE2-encoding sequence (Addgene #132775) and NG-Cas9-encoding sequence (Addgene #124163) were amplified by PCR using Phusion Polymerase (NEB). The amplicons and the linearized plasmid were assembled using an NEBuilder HiFi DNA assembly kit (NEB). The assembled plasmid was named pLenti-NG-PE2-BSD. To prepare px601-PE2, the PE2-encoding sequence (Addgene #132775) and the WPRE sequence (Addgene #52962) were amplified by PCR and cloned into the pX601 plasmid using an NEBuilder HiFi DNA assembly kit (NEB). To construct px552-pegRNA-CAG-mCherry, guide-RNA scaffold sequence (Addgene #104174) and CAG-mCherry (Addgene #108685) fragments were PCR-amplified and cloned into the px552 plasmid (Addgene #60958) to make px552-U6-CAG-mCherry. Next, pegRNA sequences were synthesized and cloned into the linearlized px552-U6-CAG-mCherry plasmid, which had been digested with SapI and SpeI (NEB), using an NEBuilder HiFi DNA assembly kit (NEB). These manipulations generated px552-pegRNA-CAG-mCherry. An sgRNA-expressing vector (Addgene #104174) was digested with BsmBI. sgRNA oligomers were annealed, phosphorylated with T4 PNK and ligated with the linearized vector to construct gN19-nicking sgRNA.

Construction of a plasmid library of pegRNA and target sequence pairs. Oligonucleotides were designed and the library of pegRNA-encoding and target sequence pairs was generated as previously described[2]. In brief, an oligonucleotide pool containing 435 pairs of *Fah* pegRNA-encoding sequences or 561 pairs of *Rpe65* pegRNA-encoding sequences and target sequences was synthesized by Twist Bioscience. Each oligonucleotide included the following elements: a 19-nt guide sequence, BsmBI restriction site 1, a 15-nt barcode stuffer sequence, BsmBI restriction site 2, the RT template sequence, the PBS, a poly T sequence, an 18-nt barcode sequence (identification barcode), and a corresponding 43- to 47-nt (*Fah*) or 49- to 89-nt (*Rpe65*)-wide target sequence that included a PAM and an RT template binding region. Oligonucleotides that contained other, unintended BsmBI sites were excluded. The barcode stuffer was later excised by digestion with BsmBI; the identification barcode (located upstream of the target sequence) allowed individual pegRNA and target sequence pairs to be identified after deep sequencing. The plasmid library containing pairs of pegRNA-encoding and target sequences was prepared using a two-step cloning process[2]. This method effectively prevents uncoupling between paired guide RNA and target sequences during PCR amplification of oligonucleotides[45].

Production of lentivirus. Eight-million HEK 293T cells were seeded on 150-mm cell culture dishes containing Dulbecco's Modified Eagle Medium (DMEM). After incubation for 16 h, the DMEM was exchanged with fresh medium containing 25 μM chloroquine diphosphate; the cells were then incubated for a further 4 h. The plasmid library, psPAX2 (Addgene #12260), and pMD2.G (Addgene #12259) were mixed to yield a total of 40 μg of the plasmid mixture. HEK 293T cells were then transfected with this mixture using polyethyleneimine. Fifteen hours later, cultures were refreshed with maintaining medium. At 48 h after transfection, the supernatant (containing lentivirus) was collected, filtered through a Millex-HV 0.45 μm low protein-binding membrane (Millipore), and aliquoted. Serial dilutions of a viral aliquot were prepared and transduced into HEK 293T cells so that the virus titre could be determined. Untransduced cells and cells treated with the serially diluted virus were both cultured in the presence of 2 μg ml^{-1} puromycin (Invitrogen). The lentiviral titre was quantified by counting the number of living cells at the time when all of the untransduced cells died as previously described[46].

Cell library generation and PE2 delivery. The cell library was generated as previously described[2]. In brief, HEK 293T cells were seeded on 18 150 mm dishes (at a density of 1.2×10^7 cells per dish) and incubated overnight. The lentiviral library was transduced into the cells at a multiplicity of infection of 0.3 to achieve >500× coverage relative to the initial number of oligonucleotides. After incubation of the cells overnight, untransduced cells were removed by maintaining the cultures in 2 μg ml^{-1} puromycin for the next 5 d. The cell library was maintained at a count of at least 7.2×10^7 cells for the entire study to preserve library diversity. Next, a total of 7.2×10^7 cells (from 6 150 mm culture dishes, each with 1.2×10^7 cells) were transfected with the pLenti-NG-PE2-BSD plasmid (80 μg per dish) using 80 μl Lipofectamine 2000 (Thermo Fisher Scientific) according to the manufacturer's instructions. Six hours later, the culture medium was replaced with DMEM supplemented with 10% fetal bovine serum and 20 μg ml^{-1} blasticidin S (InvivoGen). Five days later, the cells were collected for genomic DNA extraction.

Deep sequencing. Genomic DNA was extracted from collected cells with a Wizard genomic DNA purification kit (Promega) and from mouse tissue using a DNeasy Blood & Tissue kit (Qiagen). Target sequences were PCR-amplified using 2X Taq PCR Smart mix (SolGent). The PCR primers used for the experiment are shown in Supplementary Table 8.

In preparation for evaluating the activities of the pegRNAs in a high-throughput manner, an initial PCR included a total of 350 μg genomic DNA; assuming 10 μg genomic DNA per 10^6 cells, coverage would be more than 1,000× over the library. Genomic DNA (3.64 μg per reaction, with a total of 96 reactions) was amplified using primers that included Illumina adapter sequences, after which the products were pooled and gel-purified with a MEGAquick-spin total fragment DNA purification kit (iNtRON Biotechnology). Next, 100 ng purified DNA was amplified by PCR using primers that included barcode sequences. After gel purification, the amplicons were analysed using the NovaSeq platform (Illumina).

For evaluation of prime editing at endogenous sites, the first PCR for the amplification of the target sequence was performed in a 50 μl reaction volume that contained 3 μg of the initial genomic DNA template for liver samples and 500 ng of DNA template for retina and RPE samples. The second PCR to attach the Illumina barcode sequences was then performed using 50 ng of the purified product from the first PCR in a 30 μl reaction volume. The resulting amplicons were sequenced after gel purification using MiniSeq (Illumina) according to the manufacturer's protocols.

In experiments involving *rd12* mice, genomic DNA was extracted from the RPE with an Allprep DNA/RNA mini kit (Qiagen). The on-target *Rpe65* site and potential off-target sites were then PCR-amplified using Phusion High-Fidelity DNA Polymerase (NEB). For quantifying the prime-editing efficiency, an initial PCR was performed to amplify the target sequence in a 30 μl reaction volume that contained 50 ng of genomic DNA from the RPE. To attach Illumina index

sequences, a second round of PCR was performed using the purified product from the first PCR (50 ng) in a 30 µl reaction volume. After gel purification, the resulting amplicons were sequenced using the MiniSeq (Illumina) and MiSeq(Illumina) platforms.

Analysis of prime-editing efficiencies. Python scripts[2] were used to analyse the high-throughput results. Each pegRNA and target sequence pair was identified using a 22-nt sequence (the 18-nt barcode and 4-nt sequence located upstream of the barcode). Reads that included the specified edits but not unintended mutations within the wide target sequence were considered to contain NG-PE2-induced mutations. To exclude the background mutations generated during the oligonucleotide-synthesis and PCR amplification steps, we subtracted the background prime-editing frequencies determined in the cell library that had not been treated with NG-PE2 from the observed prime-editing frequencies as previously described[2]. pegRNA and target sequence pairs with deep sequencing read counts below 100 and those with background prime-editing frequencies above 5% were removed from the analyses as previously described[47].

To quantify the prime-editing frequencies at endogenous sites, amplicon sequences were aligned to reference sequences using Cas-analyzer[48]. The frequencies of intended and unintended edits, including substitutions and indels, were calculated as the percentage of (number of reads with the edit/number of total reads). The frequencies of such edits in the experimental groups were normalized by subtracting the average frequency of such edits in the control groups to exclude errors originating from PCR amplification and sequencing.

Generation of mutant *Fah* target sequence–containing HEK 293T cells. The target region of the *Fah* gene was PCR-amplified from genomic DNA from the *Fah*$^{mut/mut}$ mouse and cloned into a lentivirus shuttle vector derived from a hygromycin reporter plasmid[49]. Next, lentivirus was produced from the vector and transduced into HEK 293T cells at a multiplicity of infection of 0.5 so that the majority of transduced cells would have a single copy target sequence per cell. After incubation of the cells overnight, untransduced cells were removed by supplementing the culture medium with 2 µg ml^{-1} hygromycin for the next 5 d.

Mice. All animal study protocols relevant to *Fah*$^{mut/mut}$ mice were approved by the Institutional Animal Care and Use Committee (IACUC) of Yonsei University Health System (Seoul, Korea) and all animal study protocols relevant to mouse eye-related experiments were approved by the IACUC of Seoul National University and Seoul National University Hospital. *Fah*$^{mut/mut}$ mice were provided with water containing 10 mg l^{-1} NTBC unless specified. Mating pairs of *rd12* mice (stock no. 005379, The Jackson Laboratory), maintained under conditions of a 12 h:12 h dark:light cycle, produced offspring that were used for subsequent experiments. Subretinal injection was performed on the right eyes of three-week-old *rd12* mice. C57BL/6 mice, obtained from Central Laboratory Animal, were maintained under a 12 h:12 h dark:light cycle.

***Fah*$^{mut/mut}$ mice and hydrodynamic injection.** Plasmids for hydrodynamic tail-vein injection were prepared using an EndoFree Plasmid Maxi kit (Qiagen). Plasmids encoding PE2 (127 µg) and pegRNA (73 µg), which had been suspended in 2 ml normal saline, were injected into the tail vein of 5- to 7-week-old *Fah*$^{mut/mut}$ mice within 5–7 s (30 µg of sgRNA plasmid was added to the normal saline only for the PE3-treated group). For measuring the initial correction efficiency, *Fah*$^{mut/mut}$ mice were maintained on water containing NTBC for 7 d after injection with plasmid DNA; at that time, NTBC was withdrawn and a partial hepatectomy was performed. To minimize partial hepatectomy-induced hepatocyte proliferation, we removed only about 3% of the liver (10% of the median lobe). PE2-treated mice were again provided with NTBC for 5 d, from day 7 to day 12, after the initial withdrawal of NTBC at day 0; the mice were euthanized at 60 d after the initial NTBC withdrawal for histology and DNA and RNA analysis. PE3-treated mice were euthanized at 40 d after NTBC withdrawal.

AAV vector construction and virus production. To prepare the *trans*-splicing PE2 plasmid, the sequence encoding the PE2 N terminus (PE2-N term) (Addgene #132775) and a splicing donor (Addgene #112734) were PCR-amplified using primers listed in Supplementary Table 8 and cloned into the px601 plasmid using an NEBuilder HiFi DNA assembly kit (NEB). Similarly, a splicing acceptor (Addgene #112876), the sequence encoding the PE2 C terminus (PE2-C term) (Addgene #132775) and the WPRE sequence (Addgene #52962) were PCR-amplified and cloned into the pX601 plasmid using an NEBuilder HiFi DNA assembly kit (NEB).

To construct U6-*Rpe65* pegRNA-CAG-mCherry, pegRNA-encoding, sgRNA-encoding and H1 promoter sequences (Addgene #61089) were either synthesized or PCR-amplified and then cloned into the px552-U6-CAG-mCherry plasmid using an NEBuilder HiFi DNA assembly kit (NEB). The AAV vectors were then sent to VectorBuilder for packaging and ultrapurification to obtain the high-grade AAVs (serotype 8) required for an in vivo study in wild-type mice. For experiments relevant to *rd12* mice, AAV particles were produced as previously described[50]. In brief, TS-PE2-N plasmids, TS-PE2-C-WPRE plasmids or U6-*Rpe65* pegRNA-CAG-mCherry plasmids were co-transfected along with AAV2-capsid plasmids and helper plasmids into HEK 293T cells. After 3 d, cells were lysed; high-grade AAVs were then obtained via iodixanol (Optiprep, Sigma; D1556) gradient ultrapurification. Finally, viruses were concentrated in phosphate-buffered saline to obtain high-grade AAVs using a Centricon tube (Vivaspin 20, Sartorius).

Intravitreal injection of AAV. Before AAV injection, deep anaesthesia was induced by tiletamine and zolazepam (Zoletil 50, Virbac; 30 mg kg^{-1}) and xylazine (Rompun, Bayer; 10 mg kg^{-1}). Then, 4.9×10^{10} virus genomes (vg) of AAV8-TS-PE2-N term, 4.9×10^{10} vg of AAV8-TS-PE2-C term and 2.4×10^{10} vg of AAV8-Atp7b pegRNA-sgRNA in phosphate-buffered saline were mixed in a total volume of 1.5 µl and injected into the vitreous cavity of the mouse eye. A customized Nanofil syringe with a blunt 33-gauge needle (World Precision Instrument) was used for the injection, which was performed using an operating microscope (Leica).

Subretinal injection of AAV. Before injection, all mice received deep anaesthesia. Triple AAV vectors (4.76×10^{10} virus genomes (vg) for AAV-PE2-N, 4.62×10^{10} GC for AAV-PE2-C-WPRE and 2.16×10^{10} GC for pegRNA-CAG-mCherry in 3 µl phosphate-buffered saline) (Fig. 3c) were then injected into the subretinal space of mice under an operating microscope (Leica), as previously described[51]. A customized Nanofil syringe with a 33 G blunt needle (World Precision Instrument) was used for all injections.

Immunofluorescence. *Fah*$^{mut/mut}$ mice were euthanized by carbon dioxide asphyxiation. Livers were fixed in 4% paraformaldehyde overnight at 4 °C, followed by immersion in 6% sucrose overnight and immersion in 30% sucrose the next day. The livers were embedded in OCT compound (Leica), cryosectioned at 16 µm and stained with haematoxylin and eosin for pathology studies. The liver cryostat sections were washed three times with 1× phosphate-buffered saline and incubated in blocking buffer for 1 h at room temperature. The sections were then incubated with primary anti-Fah antibody (1:200, Abcam) at 4 °C overnight. After washing with 1× phosphate-buffered saline, the sections were incubated with Alexa Fluor 488 goat anti-rabbit secondary antibody (1:400, Invitrogen) for 1 h at room temperature. Cells were mounted on glass slides and nuclei were visualized using fluorescent mounting medium containing 4′,6-diamidino-2-phenylindole (DAPI; Vector). Images were captured using a confocal microscope (LSM700, Zeiss). Quantification of FAH$^+$ hepatocytes in the liver was performed for 3–5 mice per group, from >4 liver regions per mouse, with ZEN Imaging software (Blue edition, Zeiss). *rd12* mice were euthanized 6 weeks after subretinal injection and RPE-choroid-scleral tissues were obtained from enucleated eyes. Immunostaining of whole mount tissues with anti-RPE65 antibody (1:100; cat. no. NB100–355AF488, Novus) was done using standard techniques. Nuclei were stained using DAPI (Sigma). Immunostained tissues were observed using a confocal microscope (Leica).

Electroretinography. Prior to ERG, mice were kept in the dark overnight. Deep anaesthesia was induced and a Tropherin ophthalmic solution containing phenylephrine hydrochloride (5 mg ml^{-1}) and tropicamide (5 mg ml^{-1}) was administered topically to dilate pupils. A universal testing and electrophysiologic system 2000 (UTAS E-2000, LKC) was used for full-field ERG. The light-induced responses to a 0 dB Xenon flash were recorded at a gain of 2k using a notch filter at 60 Hz; responses were bandpass filtered between 0.1 and 1,500 Hz. Graphs were plotted and amplitudes were estimated using Prism 8 (GraphPad). The a-wave amplitudes were determined by measuring from the baseline to the lowest negative-going voltage and the b-wave amplitudes were measured from the a-wave trough to the highest peak of the positive b-wave.

Optomotor response. A virtual-reality optokinetic system (OptoMotry HD, CerebralMechanics) was used to measure grating acuity visual thresholds, according to the manufacturer's instructions and original publications about the system[52,53]. In brief, mice were placed on a platform where they were exposed to views of a virtual rotating cylinder on monitors surrounding the enclosure; the mice then tracked the grating with head movements. Visual thresholds were determined with a staircase procedure to produce the maximum spatial frequency (cycles/degrees) above which the mice did not respond to the rotating stimuli.

Analysis of off-target effects. Potential off-target sites were experimentally identified using Digenome-seq[17] and nDigenome-seq[18] and computationally identified using Cas-OFFinder[40] and CRISPOR[19]. For Cas-OFFinder, genomic sites containing up to 3-bp mismatches compared to the pegRNA were considered and analysed by targeted deep sequencing. From the CRISPOR results, the four top-ranking predicted off-target sites of the used pegRNA and those of the used sgRNA were selected and analysed by targeted deep sequencing. Cas-analyzer was used to analyse indel frequencies at off-target sites and the frequencies of the intended edits were analysed with the same method that was used to analyse frequencies at the on-target sites described above. The sequences of the off-target sites are provided in Supplementary Table 4. The primers used for deep sequencing are shown in Supplementary Table 8.

Digenome-seq and nDigenome-seq. Digenome-seq and nDigenome-seq are methods in which genomic DNA is treated in vitro with nuclease or nickase–sgRNA complexes and double strand or single strand break sites are identified as previously

described[17,18]. We performed Digenome-seq and nDigenome-seq as previously described[17,18]. In brief, recombinant Cas9 nuclease (100 nM, for Digenome-seq) or Cas9 H840A nickase (100 nM, for Digenome-seq) was incubated with three sgRNAs (each 100 nM, targeting *Fah*, *Rpe65* and *Atp7b*), which share guide sequences with the pegRNAs of interest, at room temperature for 10 min. Next, the resulting Cas9 nuclease or Cas9 H840A nickase–sgRNA complexes were mixed with 20 μg of genomic DNA isolated from NIH3T3 cells in a reaction buffer (100 mM NaCl, 50 mMTris–HCl, 10 mM $MgCl_2$, 100 μg ml^{-1} bovine serum albumin, at pH 7.9) and incubated for 8 h at 37 °C. Digested genomic DNA was then incubated with RNase A (50 μg ml^{-1}) and protease K to remove the sgRNA and the nuclease or nickase, after which a DNeasy tissue kit (Qiagen) was used to purify the DNA again. A Covaris system (Life Technologies) was used to shear the resulting genomic DNA (1 μg) to generate fragments of about 500 bp in size, which were then blunt-ended using End Repair Mix (illumina). To prevent self-ligation, the DNA fragments were adenylated. The fragments were then ligated with adapters using TruSeq DNA Library Prep Kits (illumina). The resulting libraries were then subjected to whole genome sequencing at a sequencing depth of 30x–40x using an Illumina HiSeq X. Issac aligner was used to align the reads to hg19. For Digenome-seq, DNA cleavage scores were calculated with previously used source codes[17] (https://github.com/chizksh/digenome-toolkit2). For nDigenome-seq, aligned sequence data were separated into forward and reverse strands and in vitro single strand break sites were analysed using previously used source code for nDigenome-seq (https://github.com/snugel/digenome-toolkit) as previously described[18]. Double- and single strand break sites with high cleavage scores were subjected to validation by targeted deep sequencing using genomic DNA extracted from mice treated with prime-editing components. All sites captured by Digenome- and nDigenome-seq are shown in Supplementary Table 4 as separate sheets.

Gene expression analysis by RT–qPCR. Total RNA was purified using TRIzol (Invitrogen) and reverse-transcribed using AccuPower RT PreMix (Bioneer). RT–qPCR was performed using SYBR Green (Applied Biosystems); the primers are listed in Supplementary Table 8. Gene expression levels were normalized to *Gapdh* levels. All experiments were performed in triplicate.

Statistics and reproducibility. *P*-values were determined by Student's *t*-test using GraphPad Prism8. To determine Pearson and Spearman correlation coefficients, we used Microsoft Excel (version 16.0, Microsoft Corporation). For high-throughput evaluation of pegRNA efficiencies, we combined the data from two replicates independently transfected by two different experimentalists.

Reporting Summary. Further information on research design is available in the Nature Research Reporting Summary linked to this article.

Data availability

The main data supporting the results in this study are available within the paper and its Supplementary Information. The deep sequencing data generated for this study are available from the NCBI Sequence Read Archive under accession numbers SRR12778000 and PRJNA732214. Source data are provided with this paper.

Received: 16 December 2020; Accepted: 21 July 2021;
Published online: 26 August 2021

References

1. Anzalone, A. V. et al. Search-and-replace genome editing without double-strand breaks or donor DNA. *Nature* **576**, 149–157 (2019).
2. Kim, H. K. et al. Predicting the efficiency of prime editing guide RNAs in human cells. *Nat. Biotechnol.* **39**, 198–206 (2021).
3. Schene, I. F. et al. Prime editing for functional repair in patient-derived disease models. *Nat. Commun.* **11**, 5352 (2020).
4. Lin, Q. et al. Prime genome editing in rice and wheat. *Nat. Biotechnol.* **38**, 582–585 (2020).
5. Liu, Y. et al. Efficient generation of mouse models with the prime editing system. *Cell Discov.* **6**, 27 (2020).
6. Paulk, N. K. et al. Adeno-associated virus gene repair corrects a mouse model of hereditary tyrosinemia in vivo. *Hepatology* **51**, 1200–1208 (2010).
7. Aponte, J. L. et al. Point mutations in the murine fumarylacetoacetate hydrolase gene: animal models for the human genetic disorder hereditary tyrosinemia type 1. *Proc. Natl Acad. Sci. USA* **98**, 641–645 (2001).
8. Yin, H. et al. Genome editing with Cas9 in adult mice corrects a disease mutation and phenotype. *Nat. Biotechnol.* **32**, 551–553 (2014).
9. Yin, H. et al. Therapeutic genome editing by combined viral and non-viral delivery of CRISPR system components in vivo. *Nat. Biotechnol.* **34**, 328–333 (2016).
10. Shin, J. H., Jung, S., Ramakrishna, S., Kim, H. H. & Lee, J. In vivo gene correction with targeted sequence substitution through microhomology-mediated end joining. *Biochem. Biophys. Res. Commun.* **502**, 116–122 (2018).
11. Song, C. Q. et al. Adenine base editing in an adult mouse model of tyrosinaemia. *Nat. Biomed. Eng.* **4**, 125–130 (2020).
12. Nishimasu, H. et al. Engineered CRISPR–Cas9 nuclease with expanded targeting space. *Science* **361**, 1259–1262 (2018).
13. Kim, N. et al. Prediction of the sequence-specific cleavage activity of Cas9 variants. *Nat. Biotechnol.* **38**, 1328–1336 (2020).
14. Kim, H. K. et al. High-throughput analysis of the activities of xCas9, SpCas9-NG and SpCas9 at matched and mismatched target sequences in human cells. *Nat. Biomed. Eng.* **4**, 111–124 (2020).
15. Kim, H. K. et al. SpCas9 activity prediction by DeepSpCas9, a deep learning-based model with high generalization performance. *Sci. Adv.* **5**, eaax9249 (2019).
16. Wilkinson, P. D. et al. The polyploid state restricts hepatocyte proliferation and liver regeneration in mice. *Hepatology* **69**, 1242–1258 (2019).
17. Kim, D. et al. Digenome-seq: genome-wide profiling of CRISPR–Cas9 off-target effects in human cells. *Nat. Methods* **12**, 237–243 (2015).
18. Kim, D. Y., Moon, S. B., Ko, J. H., Kim, Y. S. & Kim, D. Unbiased investigation of specificities of prime editing systems in human cells. *Nucleic Acids Res.* **48**, 10576–10589 (2020).
19. Haeussler, M. et al. Evaluation of off-target and on-target scoring algorithms and integration into the guide RNA selection tool CRISPOR. *Genome Biol.* **17**, 148 (2016).
20. Gao, P. et al. Prime editing in mice reveals the essentiality of a single base in driving tissue-specific gene expression. *Genome Biol.* **22**, 83 (2021).
21. Petri, K. et al. CRISPR prime editing with ribonucleoprotein complexes in zebrafish and primary human cells. *Nat. Biotechnol.* https://doi.org/10.1038/s41587-021-00901-y (2021).
22. DiCarlo, J. E., Mahajan, V. B. & Tsang, S. H. Gene therapy and genome surgery in the retina. *J. Clin. Invest.* **128**, 2177–2188 (2018).
23. Sun, L., Li, J. & Xiao, X. Overcoming adeno-associated virus vector size limitation through viral DNA heterodimerization. *Nat. Med.* **6**, 599–602 (2000).
24. Lai, Y. et al. Efficient in vivo gene expression by *trans*-splicing adeno-associated viral vectors. *Nat. Biotechnol.* **23**, 1435–1439 (2005).
25. Ryu, S. M. et al. Adenine base editing in mouse embryos and an adult mouse model of Duchenne muscular dystrophy. *Nat. Biotechnol.* **36**, 536–539 (2018).
26. Jo, D. H. et al. CRISPR–Cas9-mediated therapeutic editing of *Rpe65* ameliorates the disease phenotypes in a mouse model of Leber congenital amaurosis. *Sci. Adv.* **5**, eaax1210 (2019).
27. Cideciyan, A. V. Leber congenital amaurosis due to *RPE65* mutations and its treatment with gene therapy. *Prog. Retin. Eye Res.* **29**, 398–427 (2010).
28. Sahel, J. A. Spotlight on childhood blindness. *J. Clin. Invest.* **121**, 2145–2149 (2011).
29. Redmond, T. M. et al. Rpe65 is necessary for production of 11-*cis*-vitamin A in the retinal visual cycle. *Nat. Genet.* **20**, 344–351 (1998).
30. Russell, S. et al. Efficacy and safety of voretigene neparvovec (AAV2-hRPE65v2) in patients with *RPE65*-mediated inherited retinal dystrophy: a randomised, controlled, open-label, phase 3 trial. *Lancet* **390**, 849–860 (2017).
31. Bainbridge, J. W. B. et al. Long-term effect of gene therapy on Leber's congenital amaurosis. *N. Engl. J. Med.* **372**, 1887–1897 (2015).
32. Jacobson, S. G. et al. Improvement and decline in vision with gene therapy in childhood blindness. *N. Engl. J. Med.* **372**, 1920–1926 (2015).
33. Maeder, M. L. et al. Development of a gene-editing approach to restore vision loss in Leber congenital amaurosis type 10. *Nat. Med.* **25**, 229–233 (2019).
34. Cideciyan, A. V. et al. Effect of an intravitreal antisense oligonucleotide on vision in Leber congenital amaurosis due to a photoreceptor cilium defect. *Nat. Med* **25**, 225–228 (2019).
35. Suh, S. et al. Restoration of visual function in adult mice with an inherited retinal disease via adenine base editing. *Nat. Biomed. Eng.* **5**, 169–178 (2021).
36. Jo, D. H. et al. Therapeutic adenine base editing corrects nonsense mutation and improves visual function in a mouse model of Leber congenital amaurosis. Preprint at *bioRxiv* https://doi.org/10.1101/2021.01.07.425822 (2021).
37. Pang, J. J. et al. Retinal degeneration 12 (*rd12*): a new, spontaneously arising mouse model for human Leber congenital amaurosis (LCA). *Mol. Vis.* **11**, 152–162 (2005).
38. Kweon, J. et al. Engineered prime editors with PAM flexibility. *Mol. Ther.* **29**, 2001–2007 (2021).
39. Levy, J. M. et al. Cytosine and adenine base editing of the brain, liver, retina, heart and skeletal muscle of mice via adeno-associated viruses. *Nat. Biomed. Eng.* **4**, 97–110 (2020).
40. Bae, S., Park, J. & Kim, J. S. Cas-OFFinder: a fast and versatile algorithm that searches for potential off-target sites of Cas9 RNA-guided endonucleases. *Bioinformatics* **30**, 1473–1475 (2014).
41. Liu, P. et al. Improved prime editors enable pathogenic allele correction and cancer modelling in adult mice. *Nat. Commun.* **12**, 2121 (2021).
42. Wang, D., Tai, P. W. L. & Gao, G. Adeno-associated virus vector as a platform for gene therapy delivery. *Nat. Rev. Drug Discov.* **18**, 358–378 (2019).

43. Li, C. & Samulski, R. J. Engineering adeno-associated virus vectors for gene therapy. *Nat. Rev. Genet.* **21**, 255–272 (2020).
44. Song, M. et al. Sequence-specific prediction of the efficiencies of adenine and cytosine base editors. *Nat. Biotechnol.* **38**, 1037–1043 (2020).
45. Du, D. et al. Genetic interaction mapping in mammalian cells using CRISPR interference. *Nat. Methods* **14**, 577–580 (2017).
46. Shalem, O. et al. Genome-scale CRISPR–Cas9 knockout screening in human cells. *Science* **343**, 84–87 (2014).
47. Kim, H. K. et al. In vivo high-throughput profiling of CRISPR–Cpf1 activity. *Nat. Methods* **14**, 153–159 (2017).
48. Park, J., Lim, K., Kim, J. S. & Bae, S. Cas-analyzer: an online tool for assessing genome editing results using NGS data. *Bioinformatics* **33**, 286–288 (2017).
49. Ramakrishna, S. et al. Surrogate reporter-based enrichment of cells containing RNA-guided Cas9 nuclease-induced mutations. *Nat. Commun.* **5**, 3378 (2014).
50. Deverman, B. E. et al. Cre-dependent selection yields AAV variants for widespread gene transfer to the adult brain. *Nat. Biotechnol.* **34**, 204–209 (2016).
51. Park, S. W., Kim, J. H., Park, W. J. & Kim, J. H. Limbal approach-subretinal injection of viral vectors for gene therapy in mice retinal pigment epithelium. *J. Vis. Exp.* **102**, 53030 (2015).
52. Prusky, G. T., Alam, N. M., Beekman, S. & Douglas, R. M. Rapid quantification of adult and developing mouse spatial vision using a virtual optomotor system. *Invest Ophthalmol. Vis. Sci.* **45**, 4611–4616 (2004).
53. Douglas, R. M. et al. Independent visual threshold measurements in the two eyes of freely moving rats and mice using a virtual-reality optokinetic system. *Vis. Neurosci.* **22**, 677–684 (2005).

Acknowledgements

We thank S. Kwon and J. Park for helping with computational analyses; S. Park and Y. Kim for assisting with the experiments. This work was supported by the New Faculty Startup Fund from Seoul National University (D.H.J.); the Bio and Medical Technology Development Program of the National Research Foundation funded by the Korean government, Ministry of Science, ICT and Future Planning (NRF-2017M3A9B4062401 (H.H.K. and J.H.K.)); Brain Korea 21 Four Project for Medical Sciences (Yonsei University College of Medicine); the Basic Science Research Program through the National Research Foundation of Korea funded by the Ministry of Education (NRF-2017R1A6A3A04004741 (D.H.J.)); the Medical Research Center from the National Research Foundation of Korea (2018R1A5A2025079 (H.H.K.)); grants from the National Research Foundation of Korea (2017R1A2B3004198 (H.H.K.) and 2020R1C1C1003284 (H.H.K.)); the Creative Materials Discovery Program through the National Research Foundation of Korea (NRF-2018M3D1A1058826 (J.H.K.)); the Korea Research Institute of Bioscience and Biotechnology(KRIBB) Research Initiative Program (KGM5362111 (J.H.K)); and the Korean Health Technology R&D Project, Ministry of Health and Welfare, Republic of Korea (grant HI17C0676 (H.H.K.)).

Author contributions

H.H.K. and J.H.K. conceived and designed the study; H.J. and J.H.S. evaluated prime-editing efficiencies and analysed DNA from mice under the supervision of H.H.K.; D.H.J. and C.S.C. conducted the eye-related animal experiments under the supervision of J.H.K; H.J., J. H. Shin, G.Y. and R.G. performed the high-throughput evaluation of PE2 efficiencies; J. H. Seo and S.-R.C. conducted immunofluorescence staining and histologic evaluations related to experiments associated with *Fah*$^{mut/mut}$ mice; D.K. performed the Digenome-seq and nDigenome-seq experiments; H.H.K., D.H.J., H.J. and J.H.K. wrote the manuscript with input from all authors.

Competing interests

Yonsei University has filed a patent application based on this work and H.J. and H.H.K. are listed as inventors.

Additional information

Extended data is available for this paper at https://doi.org/10.1038/s41551-021-00788-9.

Supplementary information The online version contains supplementary material available at https://doi.org/10.1038/s41551-021-00788-9.

Correspondence and requests for materials should be addressed to J.H.K. or H.H.K.

Peer review information *Nature Biomedical Engineering* thanks the anonymous reviewer(s) for their contribution to the peer review of this work.

Reprints and permissions information is available at www.nature.com/reprints.

Publisher's note Springer Nature remains neutral with regard to jurisdictional claims in published maps and institutional affiliations.

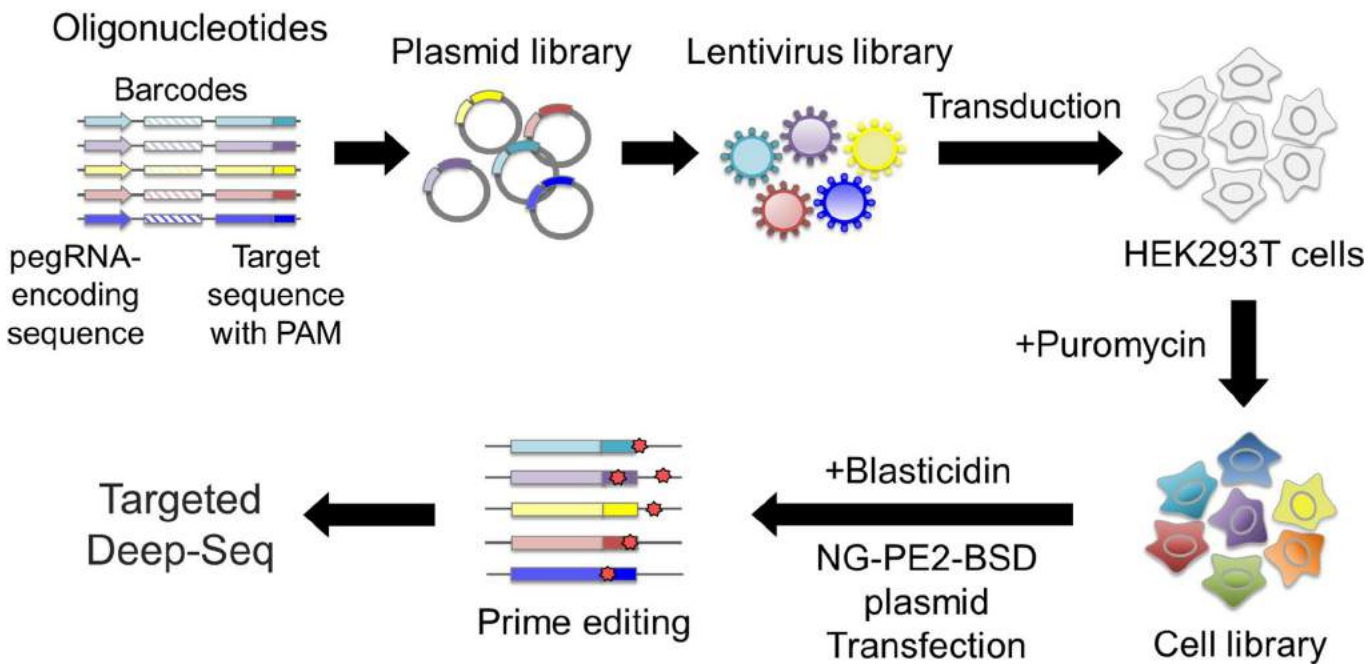

Extended Data Fig. 1 | Schematic representation of the high-throughput evaluation of pegRNA activities. A lentiviral plasmid library was prepared from a pool of oligonucleotides that contained pairs of pegRNA-encoding sequences and corresponding target sequences. Next, HEK293T cells were transduced with lentivirus generated from the plasmid library to construct a cell library and untransduced cells were removed by puromycin selection. This cell library was then transfected with a plasmid encoding NG-PE2, and untransfected cells were removed by blasticidin selection. Five days after the transfection, genomic DNA was isolated from the cells, PCR-amplified, and subjected to deep sequencing to determine prime editing efficiencies.

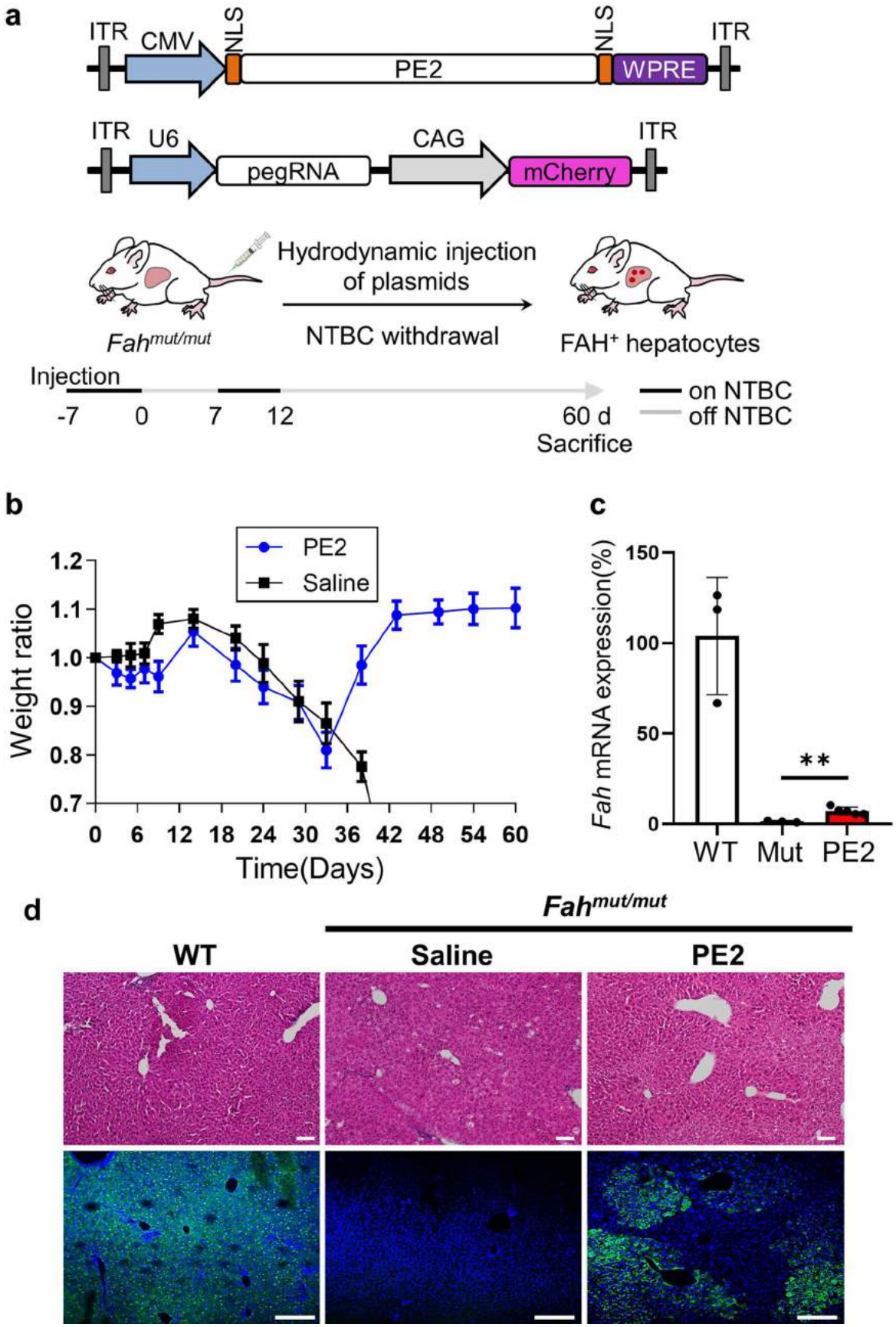

Extended Data Fig. 2 | See next page for caption.

Extended Data Fig. 2 | Prime editor 2 corrects the disease mutation and phenotype in *Fah*$^{mut/mut}$ mice. a, Maps of vectors encoding PE2 components and a schematic representation of the experiments. *Fah*$^{mut/mut}$ mice underwent injection of plasmids encoding prime editor 2 components (that is, prime editor 2 and pegRNA) and were kept on water containing NTBC for 7 days. The day on which NTBC was initially withdrawn is defined as day 0. The mice were again provided with NTBC for five days, from day 7 to day 12, after the initial withdrawal of NTBC at day 0. At 60 days, the PE2-treated mice were euthanized and analyzed. Abbreviations in the vector maps are defined in the Supplementary Figure 2 legend. **b**, Body weight of *Fah*$^{mut/mut}$ mice injected with PE2 or phosphate-buffered saline (Saline, control). Body weights were normalized to the pre-injection weight. The number of mice $n = 5$ for the PE2 group and $n = 3$ for the saline group. Data are mean ± s.e.m. **c**, The level of wild-type *Fah* mRNA in the liver measured by quantitative RT-PCR using primers that hybridize to exons 8 and 9. WT, wild-type mice; Mut, *Fah*$^{mut/mut}$ mice; PE2, *Fah*$^{mut/mut}$ mice injected with plasmids encoding PE2 components. The number of mice $n = 3$ (WT), 3 (Mut), and 5 (PE2). $^{**}P = 0.0032$. **d**, H&E staining (upper panels) and immunofluorescent staining for FAH protein (lower panels) in liver sections. Scale bars, upper panels, 100 μm; lower panels, 200 μm.

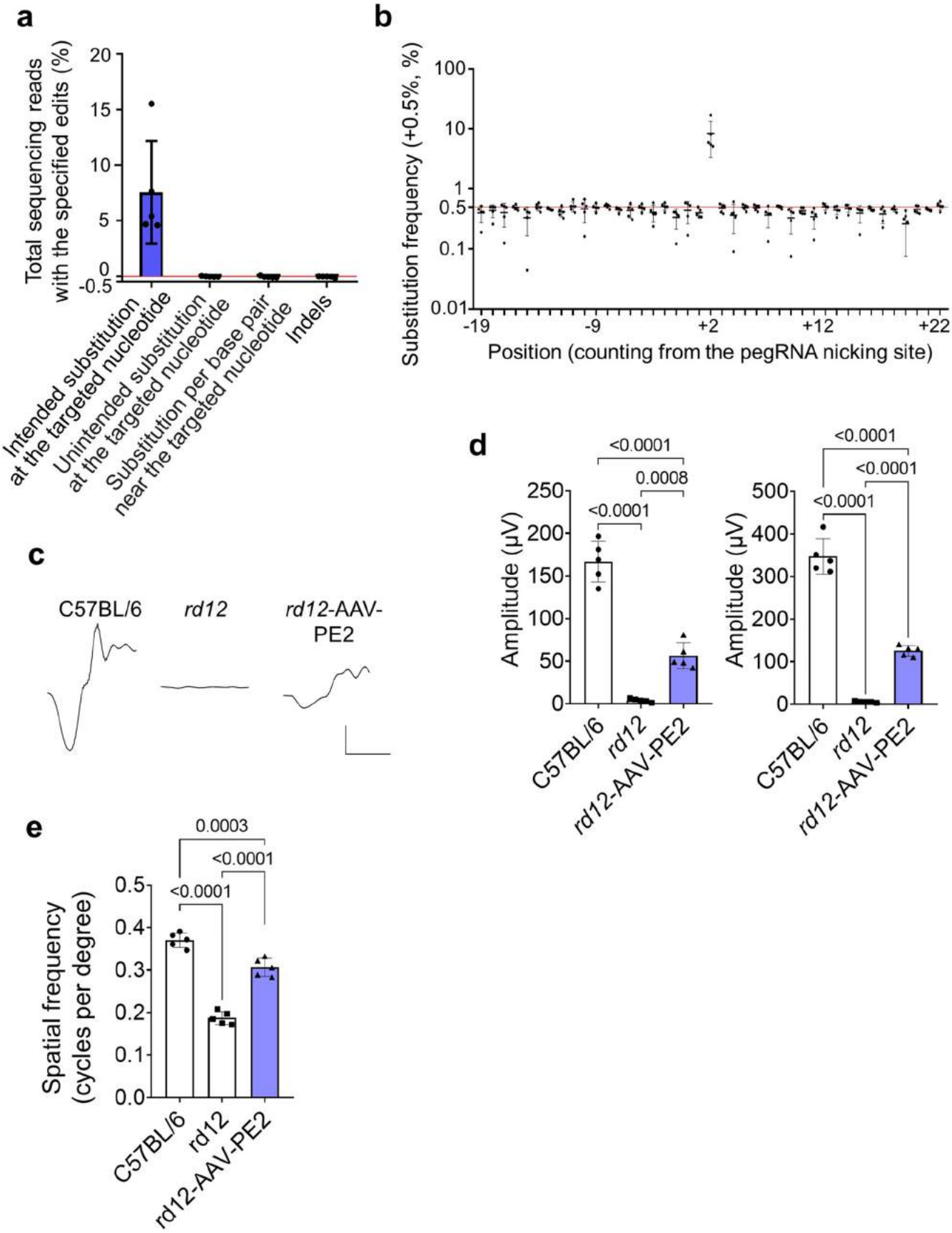

Extended Data Fig. 3 | See next page for caption.

Extended Data Fig. 3 | Correction of the LCA-causing mutation and phenotype using the most efficient pegRNA (id 157). a, Frequencies of intended and unintended edits in the RPE of AAV-PE2-treated *rd12* mice. The frequencies were normalized by subtracting the average frequency of such editing in the control group without PE2 treatment to exclude errors originating from PCR amplification and sequencing. Substitutions near the targeted nucleotide were evaluated over a 40-bp range centered on the targeted nucleotide. Indels were measured over a 60-bp range centered on the pegRNA nicking site. The red horizontal line represents the location where the normalized frequency = 0. Data are mean ± s.d. The number of mice $n = 5$. **b**, Substitution frequencies at each position of the target sequence, ranging from -20 bp to +20 bp from the targeted nucleotide, in the RPE of PE2-treated *rd12* mice. The frequencies were normalized by subtracting the average edit frequencies in the RPE of *rd12* mice without PE2 treatment to exclude errors originating from PCR amplification and sequencing. The red horizontal line represents the location where the normalized frequency = 0. Positions are numbered from the pegRNA nicking site. The targeted position is at +2. Data are mean ± s.d. The number of mice $n = 5$. **c**, Representative waveforms of dark-adapted ERG responses at 0 dB in wild-type (C57BL/6), uninjected control (*rd12)*, and *rd12* mice injected with PE2-expressing AAV (*rd12*-AAV-PE2). Scale bars, 30 ms (x-axis) and 50 μV (y-axis). **d**, Amplitudes of a-waves (left) and b-waves (right) of ERG responses of C57BL/6 and *rd12* mice. Data are mean ± s.d. The number of mice $n = 5$. *P*-values from one-way ANOVA with post-hoc Tukey's multiple comparison tests are shown. *rd12*-AAV-PE2, *rd12* mice treated with AAV-PE2. **e**, Optomotor response test results. Data are mean ± s.d. The number of mice $n = 5$. *P*-values from one-way ANOVA with post-hoc Tukey's multiple comparison tests are shown.

nature portfolio

Corresponding author(s): Jeong Hun Kim, Hyongbum Henry Kim

Last updated by author(s): Jul 16, 2021

Reporting Summary

Nature Portfolio wishes to improve the reproducibility of the work that we publish. This form provides structure for consistency and transparency in reporting. For further information on Nature Portfolio policies, see our Editorial Policies and the Editorial Policy Checklist.

Statistics

For all statistical analyses, confirm that the following items are present in the figure legend, table legend, main text, or Methods section.

n/a	Confirmed
☐	☒ The exact sample size (*n*) for each experimental group/condition, given as a discrete number and unit of measurement
☐	☒ A statement on whether measurements were taken from distinct samples or whether the same sample was measured repeatedly
☐	☒ The statistical test(s) used AND whether they are one- or two-sided *Only common tests should be described solely by name; describe more complex techniques in the Methods section.*
☒	☐ A description of all covariates tested
☐	☒ A description of any assumptions or corrections, such as tests of normality and adjustment for multiple comparisons
☐	☒ A full description of the statistical parameters including central tendency (e.g. means) or other basic estimates (e.g. regression coefficient) AND variation (e.g. standard deviation) or associated estimates of uncertainty (e.g. confidence intervals)
☐	☒ For null hypothesis testing, the test statistic (e.g. *F*, *t*, *r*) with confidence intervals, effect sizes, degrees of freedom and *P* value noted *Give P values as exact values whenever suitable.*
☒	☐ For Bayesian analysis, information on the choice of priors and Markov chain Monte Carlo settings
☐	☒ For hierarchical and complex designs, identification of the appropriate level for tests and full reporting of outcomes
☐	☒ Estimates of effect sizes (e.g. Cohen's *d*, Pearson's *r*), indicating how they were calculated

Our web collection on statistics for biologists contains articles on many of the points above.

Software and code

Policy information about availability of computer code

Data collection	NovaSeq (Illumina), Miseq (Illumina) and MiniSeq (Illumina).
Data analysis	All data were statistically analysed using GraphPad Prism 8, Microsoft Excel (version, 16.0, Microsoft Corporation). Immunofluorescence was analysed using ZEN Imaging Software (Blue edition, Zeiss).

For manuscripts utilizing custom algorithms or software that are central to the research but not yet described in published literature, software must be made available to editors and reviewers. We strongly encourage code deposition in a community repository (e.g. GitHub). See the Nature Portfolio guidelines for submitting code & software for further information.

Data

Policy information about availability of data

All manuscripts must include a data availability statement. This statement should provide the following information, where applicable:

- Accession codes, unique identifiers, or web links for publicly available datasets
- A description of any restrictions on data availability
- For clinical datasets or third party data, please ensure that the statement adheres to our policy

The main data supporting the results in this study are available within the paper and its Supplementary Information. The deep-sequencing data generated for this study are available from the NCBI Sequence Read Archive under accession numbers SRR12778000 and PRJNA732214. Unprocessed gel images associated with Fig. 3c are provided as Source data.

Field-specific reporting

Please select the one below that is the best fit for your research. If you are not sure, read the appropriate sections before making your selection.

☒ Life sciences ☐ Behavioural & social sciences ☐ Ecological, evolutionary & environmental sciences

For a reference copy of the document with all sections, see nature.com/documents/nr-reporting-summary-flat.pdf

Life sciences study design

All studies must disclose on these points even when the disclosure is negative.

Sample size	No statistical methods were used to predetermine sample sizes. For the animal experiments, we described the sample sizes in the relevant figure legends. All sample sizes were chosen on the basis of previous experience with similar experiments, and were sufficient according to the statistical tests performed.
Data exclusions	For the high-throughput evaluatation of pegRNA activities, pegRNAs with deep-sequencing read counts below 100 or background prime-editing frequencies above 5% were excluded, to increase the accuracy of the analysis.
Replication	The high-throughput evaluation of prime-editing efficiencies were independently repeated twice, with similar results. Individual evaluations of prime-editing efficiencies of pegRNAs were performed three-times by independent transfections, with comparable results. All experiments involving animals were performed in at least three independent mice, with reproducible results.
Randomization	Mice were randomly allocated into experimental or control groups. For all studies, samples and organisms were randomly allocated to the experimental groups.
Blinding	Blinding was not relevant to the study.

Reporting for specific materials, systems and methods

We require information from authors about some types of materials, experimental systems and methods used in many studies. Here, indicate whether each material, system or method listed is relevant to your study. If you are not sure if a list item applies to your research, read the appropriate section before selecting a response.

Materials & experimental systems

n/a	Involved in the study
☐	☒ Antibodies
☐	☒ Eukaryotic cell lines
☒	☐ Palaeontology and archaeology
☐	☒ Animals and other organisms
☒	☐ Human research participants
☒	☐ Clinical data
☒	☐ Dual use research of concern

Methods

n/a	Involved in the study
☒	☐ ChIP-seq
☒	☐ Flow cytometry
☒	☐ MRI-based neuroimaging

Antibodies

Antibodies used	Anti-Fumarylacetoacetate hydrolase antibody (ab81087) Alexa Fluor® 488 goat anti-Rabbit(A-11008) Anti-RPE65 antibody (cat. no. NB100-355AF488, Novus) at 1:100 dilution.
Validation	Anti-Fumarylacetoacetate hydrolase antibody, IHC 1:200 Alexa Fluor® 488 goat anti-Rabbit antibody, IHC 1:400 Vendor information: https://www.novusbio.com/products/rpe65-antibody-4018b113d9_nb100-355af488 https://www.novusbio.com/products/rpe65-antibody-4018b113d9_nb100-355 Novus website provides an image of immunofluorsecence studies on mouse retinal tissues. Mouse monoclonal antibodies to bovine RPE65 microsomal membrane proteins. CiteAb finds 55 citations for this antibody: https://www.citeab.com/antibodies/408298-nb100-355-rpe65-antibody-401-8b11-3d9?des=7d7ec5ad888832fe

Eukaryotic cell lines

Policy information about cell lines

Cell line source(s)	The HEK293T, Neuro2A and NIH3T3 cells were provided by American Type Culture Collection (ATCC).

Authentication	HEK293T, Neuro2A, and NIH3T3 cells were authenticated by the supplier.
Mycoplasma contamination	The cell lines were not tested for mycoplasma contamination.
Commonly misidentified lines (See ICLAC register)	No commonly misidentified cell lines were used.

Animals and other organisms

Policy information about studies involving animals; ARRIVE guidelines recommended for reporting animal research

Laboratory animals	5–7-week-old Fah mut/mut mice were used as a mouse model of tyrosinemia. C57BL/6 mice were used for the intravitreal injection of AAVs. C57BL/6 (control mice) and rd12 mice (3-week-old, mixed gender) were used as a mouse model of Leber congenital amaurosis.
Wild animals	The study did not involve wild animals.
Field-collected samples	The study did not involve samples collected from the field.
Ethics oversight	Institutional Animal Care and Use Committee of Yonsei University Health System, and Institutional Animal Care and Use Committees of both Seoul National University and Seoul National University Hospital.

Note that full information on the approval of the study protocol must also be provided in the manuscript.